Pm. IAU COSPAR Sym on
Physics of Compact Objects
Theory vs Observation
Sofia July 1987
Bulgaria

High Energy X-ray Timing and Spectral Observations of Sco X-1, Cyg X-1, GX 5-1, Cyg X-3 and GX 1+4

S.V. Damle[1], P.K. Kunte[1], D.A. Leahy[2],
S. Naranan[1], B.V. Sreekantan[1] and D. Venkatesan[2]

[1] Tata Institute of Fundamental Research, Bombay - 400 005 (India)
[2] Dept. of Physics, The University of Calgary, Calgary (Canada)

Abstract

A high energy X-ray astronomy payload with phoswich scintillation detectors was flown from Hyderabad, India on December 18, 1984. Five galactic X-ray sources, Sco X-1, Cyg X-1, GX 5-1, Cyg X-3 and GX 1+4 were osberved. The timing data, with a high time resolution of 40 μs, were analysed for periodicities and quasi-periodic oscillations (QPO's). GX 1+4 was in a low luminosity state and showed pulsations with a period of 95.9 s. Its period derivative was calculated. Sco X-1 was found not to exhibit QPO's in 18-40 keV X-rays with a 90% confidence limit of 0.20 on amplitude. Spectra are presented for Sco X-1, Cyg X-1 and GX 5-1.

1. INTRODUCTION

An X-ray astronomy telescope was launched from the Tata Institute of Fundamental Research (TIFR) Balloon Facility near Hyderabad, India on December 18, 1984. The balloon was at the float altitude from 08-50 to 16-30 hours, Indian Standard Time (IST). (UT is 5.5 hours earlier than IST). Seven galactic X-ray sources were tracked with exposures ranging from 20 minutes to 2 hours. The five sources, Sco X-1, Cyg X-1, GX 5-1, Cyg X-3 and GX 1+4 were observed. The results are presented in this paper.

Four phoswich detectors with 3 mm NaI(Tl) and 25 mm CsI(Na) crystal scintillators had a total effective area of 330 cm^2. Each detector had a field of view of 5° x 5° FWHM defined by a brass collimator and was surrounded by a passive graded shield of lead, tin, copper. Each phoswich was coupled to a 12.5 cm diameter photomultiplier tube. Pulse-height and pulse-width for every detected event was telemetered in 128 channels each, along with photon arrival time, telescope elevation and azimuth and house-keeping information (e.g. pressure, temperature, instrument voltages etc.) Particle and gamma-ray (non X-ray) events were rejected by pulse-width discrimination. Event times were determined with a resolution of 40 μs. The rms accuracy of the pointing of the alt -azimuth mounted telescope was 0.35°. The telescope was pre-programmed to track the X-ray sources in elevation and azimuth. Because of the low signal to background rates, roughly equal times were spent on observing "source + background" and "background" in the same range of telescope elevation and azimuth, for optimum determination of "signal". In-flight calibration was performed by exposing the detectors periodically to an Am^{241} radioactive source to monitor the stability of detectors and the associated electronics. The telemetry rate was one frame of 32 eight-bit words every 5.12 ms (50 kbs). Details of detectors and instrumentation are given by Damle et al. (1986).

Table 1 : Count Rate Summary

Source	Sco X-1	Cyg X-1	GX 5-1	Cyg X-3	GX 1+4
Observation Time (s)	2310	625	2038	2429	5745
Energy Range (keV)	18-60	18-120	18-100	18-80	18-60
Count Rate (in 10^{-3} cm^{-2} s^{-1})	8.74 (0.30)	24.6 (0.79)	4.01 (0.42)	2.54 (0.62)	1.05 (0.22)

2. OBSERVATIONS AND DATA ANALYSIS

Pulse-width discrimination eliminated nearly 85% of the events as non X-ray background. A summary of the count rates obtained from the five sources after subtracting background ("source + background" - "background") is given in Table 1. The rates are corrected for dead time (10%). The numbers in parentheses are one sigma errors.

Source Spectra

The primary spectrum at the top of the atmosphere (in photons cm^{-2} s^{-1} keV^{-1}) for each source can be obtained from the observed pulse-height distribution by (1) deconvolving the detector response function and (2) correcting for atmospheric absorption. (The over-lying atmosphere in the direction of X-ray sources varied from 4.31 to 5.42 g cm^{-2}). However, the procedure is feasible only if a form of the primary spectrum is specified. Normally two types of primary spectra are assumed : a power-law spectrum and thermal bremsstrahlung from an optically thin plasma. We have included a third : a Comptonized black-body spectrum (Syunyaev and Titarchuk, 1980).

The primary photon spectrum is transformed into a pulse-height distribution at the appropriate atmospheric depth taking into account the variation with energy of atmospheric absorption and the detector response function. The latter included the experimentally determined detector (Gaussian) response and the effects of the escape of Iodine K_α and K_β

X-rays from the phoswich detector for incident X-rays above the K-electron binding energy. For an assumed primary spectrum, (in other words a given choice of parameters of the spectrum), we calculate the count rates in pulse-height channels corresponding to energy intervals 18-25, 25-40, 40-60, 60-80, 80-100 and 100-120 keV, for comparison with the observed count rates. A χ^2- test determines the best-fit parameters for the primary spectrum and the statistical errors. Further details on the procedure can be found in Damle et al. (1987).

The best-fit model spectra for Sco X-1, GX 5-1 and Cyg X-1 are presented in Table 2. In Fig.1 the spectra of Cyg X-1 (open circles) and GX 5-1 (filled circles) are shown and in Fig.2 the spectrum of Sco X-1.

Table 2 : Spectral parameters

X-ray Source	Sco X-1	GX 5-1	Cyg X-1
Spectral Model F(E) (ph/cm^{2}s keV)	Thermal Brems $\frac{Ae^{-E/Eo}}{E}$ G(E) $G(E) = 0.9\left(\frac{E}{Eo}\right)^{\alpha}$ $\alpha = 0.37\left(\frac{30}{Eo}\right)^{0.15}$	Power Law $AE^{-\gamma}$	Comptonized black-body $Ax^{-\alpha}e^{-x}\int_0^{\infty} t^{\alpha-1}e^{-t}(x+t)^{\alpha+3}dt$ $x=E/E_o$, $\alpha=\sqrt{\gamma+2.25}-1.5$ $\gamma=\frac{K}{E_o(\tau+2/3)^2}$ K = 1681 (sphere), 420(disc)
Best fit parameters			
Constant A	15.9	0.51	3.09×10^{-4}
Temperature E_o (keV)	6.5 ± 0.9	-	28 ± 4
Index γ	-	2.00 ± 0.51	-
Optical depth τ	-	-	6.0 (sphere), 2.7 (disc)
Total Flux (ph/cm^{2}s) (Energy interval in keV)	0.165 ± .006 (18-40)	$(2.26 \pm 0.34)10^{-2}$ (18-100)	$(8.43 \pm 0.43)\ 10^{-2}$ (18-120)

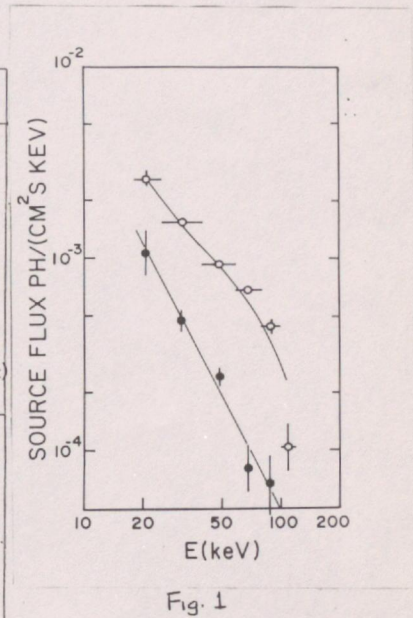

Fig. 1

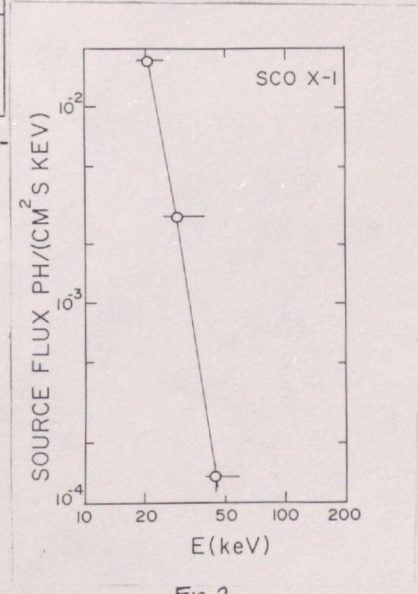

Fig. 2

In the Comptonized black-body spectrum, Eo (=kTe) is the plasma electron temperature and τ the Thompson optical depth for electron scattering for spherical or disc shaped plasmas. Because of low statistics, only total fluxes could be determined for Cyg X-3 and GX 1+4.

Cyg X-3 : Flux (25-80 keV) = $(8.67 \pm 2.33)\ 10^{-3}$ ph/cm^2 s

GX 1+4 : Flux (18-60 keV) = $(7.33 \pm 2.24)\ 10^{-3}$ ph/cm^{2}s

Timing Analysis

The timing analysis consisted of first converting the telemetry data to photon arrival times and then of analyzing the arrival times. Fast Fourier transforms (FFT's) were performed on the timing data to test for periodicities or QPO's. The epoch folding technique was employed to search for periodicity when the period was known to be restricted to a narrow range (e.g. for GX 1+4). A description of the FFT and epoch folding methods can be found in Leahy et al. (1983). Units of power are normalized in all calculations to be dimensionless and have the same scale as chi-squared. For the observed sources the background signal is several times the source signal. This results in 90% confidence limits on amplitudes for periodic signals which are greater than 0.20 when expressed as a fraction of source signal. Only for GX 1+4 was any periodicity detected. For the other sources upper limits on the presence of periodicities were determined. For GX 1+4 the epoch folding technique was applied to accurately determine the pulse period, and to produce a light curve.

Simulations were run to test that the FFT and epoch folding programs were performing correctly. Simulated photon arrival times were created using a time bin of 4×10^{-3} s, count rate of 11.103 s^{-1} (typical of these observations), and with Poisson-distributed time intervals. FFT's were performed on the simulated data with number of time bins in the range 2^{13} to 2^{23}. In all tested cases the power was χ^2 distributed (2 degrees of freedom). For example for the 2^{23} bin FFT the expected number of frequencies with power greater than 25.0 is 15.5, the simulation had 14.

The 5.12 ms telemetry frame period causes a variable dead time, i.e., no events are recorded between the first event to occur in a frame and the end of that frame. Due to the low count rates (of order 10 s^{-1}), the deadtime does

not have a significant effect. A 5.12 ms periodicity occurs in all data due to the method used in the initial analysis, thus all results given here are limited to periods greater than 5.12 ms. A reanalysis in progress will correct this. The results of this new analysis will be valid up to the full time resolution of the data of 0.04 milliseconds.

FFT's were performed on continuous spans of on-source data and in addition to spans of off-source data. In Table 3 are given the longest continuous data spans for each source together with the energy range corresponding to the pulse height channels chosen for analysis, the total number of events in each data span, and the start and stop times in IST.

Table 3 : Data Sets for FFT Analysis

X-ray Source	Energy Range (keV)	No. of events	Time span (IST) START	STOP
Sco X-1	18-40	18226	09:42:25	10:19:00
Cyg X-1	18-120	17330	15:08:29	15:18:00
Cyg X-3	18-80	7768	15:32:00	15:43:39
GX 5-1	18-100	30568	13:37:30	14:01:32
GX 1+4	18-60	24415	11:34:00	12:11:00

The resulting limits on the amplitude of any periodic signal are summarized in Table 4. The number of bins used for the FFT, the maximum frequency and the 90% confidence limits on amplitude are given. No periodicities were detected, nor were any QPO's seen in any of these sources. This however does not conflict with the results obtained at lower energies since the amplitude limits obtained here are large (greater than 20%)

Table 4 : FFT Limits on Periodicities

X-ray Source	No. of bins	Maximum frequency	Amplitude fraction (90% confidence limit) of Total Flux	of Source Flux
Sco X-1	2^{13}	1.9515	0.052	0.20
	2^{13}	100.00	0.097 (53x40.96s ffts)	0.37
	2^{13}	1000.0	0.189 (532x4.096s ffts)	0.72
Cyg X-1	2^{16}	57.437	0.059	0.30
Cyg X-3	2^{13}	5.8598	0.078	0.20
GX 5-1	2^{16}	22.724	0.044	0.84
GX 1+4	2^{16}	14.76	0.05	1.80

For GX 1+4, the 90% confidence limit amplitude as fraction of source flux exceeds 1.0 indicating that FFT is of no avail to detect any period in the source.

Epoch folding was done on all the data on GX 1+4 (5340 s of "on source" time between 10:37 and 13:37 IST) for 40 periods between 94.2 and 98.2 s and for 40 periods between 186 and 198 s. A maximum χ^2 of 16.03 (for 8 bins) was found for the period of 96.2 s. A fit of theoretical χ^2 vs. period to the observed relation (Leahy, 1987) gave a

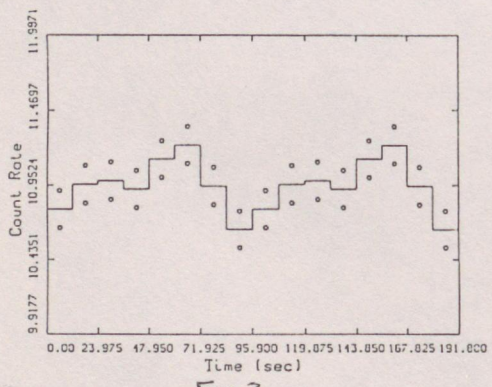

Fig. 3

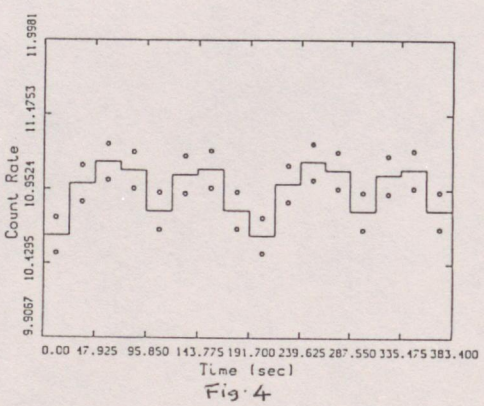

Fig. 4

best-fit period 95.9 (0.12) s and amplitude a=0.015(0.0025), where the 90% error is given in brackets. A maximum χ^2 of 14.33 was found for the period of 191.7 s. A fit of theoretical χ^2 vs. period to the observed relation gave a best-fit period 191.7 (0.7)s and amplitude a=0.010 (0.004). The light curves at 95.9 s and 191.7 s are plotted in Fig. 3, 4 with $\pm 1\sigma$ errors plotted as small circles. We cannot determine whether the shorter or longer period is the neutron star rotation period, however the shorter (96 s) period has greater statistical significance.

3. DISCUSSION AND CONCLUSIONS

Sco X-1 and Cyg X-1 are known to be highly variable in low energy as well as high energy X-rays. The measured temperature of the optically thin plasma of Sco X-1 (E_o = kT= 6.5 ± 0.9 keV) is within the range of variability seen (Soong and Rothschild, 1983). Cyg X-1 shows a complex time variability, and at least two modes, called the high and low state (see E.P. Liang and P.L. Nolan, 1984 for a recent review). As noted in several earlier observations, the spectrum begins to steepen (from a power-law spectrum) in 50-100 keV (Fig.1). Steinle et al (1982) have hard X-ray balloon data of high statistical accuracy from Cyg X-1 (Sep 24, 1977) when it was in a low state. Their results are best fit by a Comptonized black-body spectrum with A = 7.4 x 10^{-4}, E_o = 29.2 keV and τ = 5.1 (sphere). Comparing with our model parameters (Table 2) we note that while the temperature and Thompson optical depths are comparable in the two spectra, the absolute flux in the present experiment (1984) is about 0.4 times the 1977 fluxes. Further, our results (Fig.1) seem to indicate a decline in flux above 100 keV steeper than the best-fit Comptonized spectrum.

The X-ray binary pulsar GX 1+4, is one of the brightest known hard X-ray sources, but was in a low state. The last reported pulsar period measurements were in 1979 and based on the period history in 1974-79, Elsner et al (1985) deduced a period derivative $\dot{P}$ = -2.681 ± 0.096 s/y. The present period (95.9 s) nearly six years after the last measurement gives a $\dot{P}$ =-2.939 ± .022 s/y. The observed amplitude indicates that nearly 50% of X-rays from GX 1+4 in 18-60 keV are pulsed.

ACKNOWLEDGEMENTS

D.A. Leahy and D. Venkatesan acknowledge support from Natural Sciences and Engineering Research Council grants 69-0366 and 69-1565 (resp.) and acknowledge the Space Research Facilities Board/National Research Council (Space Division/ NRC, Ottawa) for support in the form of balloons. We wish to thank the following : A.T. Kothare, J.P. Malkar and J.G. Devdhekar for building the payload and intrumentation, A.V. John for help in computation and the staff of the Balloon Facility, Hyderabad for the successful balloon launch. We wish to acknowledge useful discussions with Dr. D. Narasimha.

REFERENCES

Damle, S.V., Kothare, A.T., Kunte, P., Malkar, J.P., Naranan, S., Sreekantan, B.V., Venkatesan, D. "A High Sensitivity Phoswich Scintillator X-Ray Teleścope for Hard X-Ray (20-120 keV) Astronomy from Balloon Platform" 1986, Proceedings of XXVI COSPAR 86, Toulouse June 30-July 11, 1986.

Damle, S.V., Kunte, P.K., Naranan, S., Sreekantan, B.V., and Venkatesan, D.V. "Hard X-ray Observations of the quasar 3C273" : To appear in Astron. Astrophys. Letters (1987)

Elsner, R.F., Weisskopf, M.C., Apparao, K.M.V., Darbro, W., Ramsey, B.D., Williams, A.C., Grindlay, J.E., and Sutherland, P.G., "X-ray observations of GX 1+4 with the Monitor Proportional Counter on board the EINSTEIN Observatory". 1985, The Astrophys. J., 297, 288

Leahy, D.A., Darbro, W., Elsner, R.F., Weisskopf, M.C., Sutherland, P.G., Kahn, S., Grindlay, J.E., "On Searches for Pulsed Emission with Application to Four Globular Cluster X-ray Sources : NGC 1851, 6641, 6624, and 6712" 1983, Ap.J. 266, 160.

Leahy, D.A. "On Searches for Pulsed Emission: Improved Determination of Period and Amplitude from Epoch Folding for Sinusoidal Signals" 1987, Astron. Ap. (to appear).

Liang, E.P., and Nolan, P.L. "Cygnus X-1 revisited " : 1984, Space Science Reviews, 38, 353.

Soong, Y., and Rothschild, E. "Long-term, Hard X-rays Observations of Sco X-1 from HEAO-1" : 1983, Astrophys. J., 274, 327

Steinle, H., Voges, W., Pietsch, W., Reppin, C., Trümper, J., Kendziora, E. and Staubert, R. "The Hard X-ray Spectrum of Cygnus X-1" : 1982, Astron. Astrophys., 107, 350

Syunyaev, R.A. and Titarchuk, L.G. "Comptonization of X-rays in Plasma Clouds" : 1980, Astron. Astrophys., 86, 121.

Adv. Space Res. Vol. 8, No. 2-3, pp. (2)415-(2)419, 1988
Printed in Great Britain.

0273-1177/88 $0.00 + .50

HIGH ENERGY X-RAY TIMING AND SPECTRAL OBSERVATIONS OF SCO X-1, CYG X-1, GX 5-1, CYG X-3 AND GX 1+4

S. V. Damle,* P. K. Kunte,* D. A. Leahy,** S. Naranan,*
B. V. Sreekantan* and D. Venkatesan**

*Tata Institute of Fundamental Research, Bombay – 400 005, India
**Department of Physics, The University of Calgary, Calgary, Alberta, Canada

ABSTRACT

A high energy X-ray astronomy payload with phoswich scintillation detectors was flown from Hyderabad, India on December 18, 1984. Five galactic X-ray sources, Sco X-1, Cyg X-1, GX 5-1, Cyg X-3 and GX 1+4 were observed. The timing data, with a high time resolution of 40 μs, were analysed for periodicities and quasi-periodic oscillations (QPO's). GX 1+4 was in a low luminosity state and showed pulsations with a period of 95.9 s. Its period derivative was calculated. Sco X-1 was found not to exhibit QPO's in 18-40 keV X-rays with a 90% confidence limit of 0.20 on amplitude. Spectra are presented for Sco X-1, Cyg X-1 and GX 5-1.

INTRODUCTION

An X-ray astronomy telescope was launched from the Tata Institute of Fundamental Research (TIFR) Balloon Facility near Hyderabad, India on December 18, 1984. The balloon was at the float altitude from 08:50 to 16:30 hours, Indian Standard Time (IST). (UT is 5.5 hours earlier than IST). Seven galactic X-ray sources were tracked with exposures ranging from 20 minutes to 2 hours. The five sources, Sco X-1, Cyg X-1, GX 5-1, Cyg X-3 and GX 1+4 were observed. The results are presented in this paper.

Four phoswich detectors with 3 mm NaI(Tl) and 25 mm CsI(Na) crystal scintillators had a total effective area of 330 cm^2. Each detector had a field of view of 5° x 5° FWHM defined by a brass collimator and was surrounded by a passive graded shield of lead, tin, copper. Each phoswich was coupled to a 12.5 cm diameter photomultiplier tube. Pulse-height and pulse-width for every detected event was telemetered in 128 channels each, along with photon arrival time, telescope elevation and azimuth and house-keeping information (e.g. pressure, temperature, instrument voltages, etc.). Particle and gamma-ray (non X-ray) events were rejected by pulse-width discrimination. Event times were determined with a resolution of 40 μs. The rms accuracy of the pointing of the alt-azimuth mounted telescope was 0.35°. The telescope was preprogrammed to track the X-ray sources in elevation and azimuth. Because of the low signal to background rates, roughly equal times were spent on observing "source + background" and "background" in the same range of telescope elevation and azimuth, for optimum determination of "signal". In-flight calibration was performed by exposing the detectors periodically to an Am^{241} radioactive source to monitor the stability of detectors and the associated electronics. The telemetry rate was one frame of 32 eight-bit words every 5.12 ms (50 kbs). Details of detectors and instrumentation are given in /1/.

TABLE 1 Count Rate Summary

Source	Sco X-1	Cyg X-1	GX 5-1	Cyg X-3	GX 1+4
Observation Time (s)	2310	625	2038	2429	5745
Energy Range (keV)	18-60	18-120	18-100	18-80	18-60
Count Rate (in 10^{-3} cm^{-2} s^{-1})	8.74 (0.30)	24.6 (0.79)	4.01 (0.42)	2.54 (0.62)	1.05 (0.22)

OBSERVATIONS AND DATA ANALYSIS

Pulse-width discrimination eliminated nearly 85% of the events as non X-ray background. A summary of the count rates obtained from the five sources after subtracting background ("source + background" - "background") is given in Table 1. The rates are corrected for dead-time (10%). The numbers in parentheses are one sigma errors.

Source Spectra

The primary spectrum at the top of the atmosphere (in photons $cm^{-2}s^{-1}keV^{-1}$) for each source can be obtained from the observed pulse-height distribution by (1) deconvolving the detector response function and (2) correcting for atmospheric absorption. (The over-lying atmosphere in the direction of X-ray sources varied from 4.31 to 5.42 g cm^{-2}). However, the precedure is feasible only if a form of the primary spectrum is specified. Normally two types of primary spectra are assumed; a power-law spectrum and thermal bremsstrahlung from an optically thin plasma. We have included a third: a Comptonized black-body spectrum /2/.

The primary photon spectrum is transformed into a pulse-height distribution at the appropriate atmospheric depth taking into account the variation with energy of atmospheric absorption and the detector response function. The latter included the experimentally determined detector (Gaussian) response and the effects of the escape of Iodine K_α and K_β X-rays from the phoswich detector for incident X-rays above the K-electron binding energy. For an assumed primary spectrum, (in other words a given choice of parameters of the spectrum), we calculate the count rates in pulse-height channels corresponding to energy intervals 18-25, 25-40, 40-60, 60-80, 80-100 and 100-120 keV, for comparison with the observed count rates. A χ^2-test determines the best-fit parameters for the primary spectrum and the statistical errors. Further details of the procedure can be found in /3/.

The best-fit model spectra for Sco X-1, GX 5-1, and Cyg X-1 are presented in Table 2. In Fig. 1 the spectra of Cyg X-1 (open circles) and GX 5-1 (filled circles) are shown and in Fig. 2 the spectrum of Sco X-1.

TABLE 2 Spectral Parameters

X-ray Source:	Sco X-1	GX 5-1	Cyg X-1
Spectral Model:	Thermal Brems	Power Law	Comptonized black-body
F(E) (ph/cm^2s keV):	$\frac{Ae^{-E/Eo}}{E} G(E)$	$AE^{-\gamma}$	$Ax^{-\alpha}e^{-x}\int_0^\infty t^{\alpha-1}e^{-t}(x+t)^{\alpha+3}dt$
	$G(E) = 0.9\left(\frac{E}{Eo}\right)^{\alpha}$		$x = E/E_o$, $\alpha = \sqrt{\gamma+2.25}-1.5$
	$\alpha = 0.37\left(\frac{30}{Eo}\right)^{0.15}$		$\gamma = \frac{K}{E_o(\tau+2/3)^2}$
			K = 1681 (sphere), 420 (disc)
Best fit parameters			
Constant A:	15.9	0.51	3.09×10^{-4}
Temperature E_o (keV):	6.5 ± 0.9	-	28 ± 4
Index: γ	-	2.00 ± 0.51	-
Optical depth: τ	-	-	6.0 (sphere), 2.7 (disc)
Total Flux (ph/cm^2s):	0.165 ± .006	$(2.26 \pm 0.34)10^{-2}$	$(8.43 \pm 0.43)\ 10^{-2}$
Energy interval in keV:	18-40	18-100	18-120

In the Comptonized black-body spectrum, Eo (=kTe) is the plasma electron temperature and τ the Thompson optical depth for electron scattering for spherical or disc shaped plasmas. Because of low statistics, only total fluxes could be determined for Cyg X-3 and GX 1+4.

Cyg X-3: Flux (25-80 keV) = $(8.67 \pm 2.33)\ 10^{-3}$ ph/cm^{2}s
GX 1+4: Flux (18-60 keV) = $(7.33 \pm 2.24)\ 10^{-3}$ ph/cm^{2}s

Timing Analysis

The timing analysis consisted of first converting the telemetry data to photon arrival times and then of analyzing the arrival times. Fast Fourier transforms (FFT's) were performed on the timing data to test for periodicities or QPO's. The epoch folding technique was employed to search for periodicity when the period was known to be restricted to a narrow range (e.g. for GX 1+4). A description of the FFT and epoch folding methods can be found in /4/. Units of power are normalized in all calculations to be dimensionless and have the same scale as chi-squared. For the observed sources the background signal is several times the source signal. This results in 90% confidence limits on amplitudes for periodic signals which are greater than 0.20 when expressed as a fraction of source signal. Only for GX 1+4 was any periodicity detected. For the other sources upper limits on the presence of periodicities were determined. For GX 1+4 the epoch folding technique was applied to accurately determine the pulse period, and to produce a light curve.

Simulations were run to test that the FFT and epoch folding programmes were performing correctly. Simulated photon arrival times were created using a time bin of 4×10^{-5} s, count rate of 11.103 s^{-1} (typical of these observations), and with Poisson-distributed time intervals. FFT's were performed on the simulated data with number of time bins in the range 2^{13} to 2^{23}. In all tested cases the power was χ^2 distributed (2 degrees of freedom). For example for the 2^{23} bin FFT the expected number of frequencies with power greater than 25.0 is 15.5, the simulation had 14.

The 5.12 ms telemetry frame period causes a variable dead time, i.e., no events are recorded between the first event to occur in a frame and the end of that frame. Due to the low count rates (of order 10s^{-1}), the deadtime does not have a significant effect. A 5.12 ms periodicity occurs in all data due to the method used in the initial analysis, thus all results given here are limited to periods greater than 5.12 ms. A reanalysis in progress will correct this. The results of this new analysis will be valid up to the full time resolution of the data of 0.04 milliseconds.

FFT's were performed on continuous spans of on-source data and in addition to spans of off-source data. In Table 3 are given the longest continuous data spans for each source together with the energy range corresponding to the pulse height channels chosen for analysis, the total number of events in each data span, and the start and stop times in IST.

TABLE 3 Data Sets for FFT Analysis

X-ray Source	Energy Range (keV)	No. of events	Time span (IST) START	STOP
Sco X-1	18-40	18226	09:42:25	10:19:00
Cyg X-1	18-120	17330	15:08:29	15:18:00
Cyg X-3	18-80	7768	15:32:00	15:43:39
GX 5-1	18-100	30568	13:37:30	14:01:32
GX 1+4	18-60	24415	11:34:00	12:11:00

The resulting limits on the amplitude of any periodic signal are summarized in Table 4. The number of bins used for the FFT, the maximum frequency and the 90% confidence limits on amplitude are given. No periodicities were detected, nor were any QPO's seen in any of these sources. This however does not conflict with the results obtained at lower energies since the amplitude limits obtained here are large (greater than 20%).

TABLE 4 FFT Limits on Periodicities

X-ray Source	No. of bins	Maximum Frequency	Amplitude Function (90% confidence limit) of Total Flux	of Source Flux
Sco X-1	2^{13}	1.866	0.052	0.20
	2^{13}	100.00	0.097 (53 x 40.96s ffts)	0.37
	2^{13}	1000.0	0.189 (532 x 4.096s ffts)	0.72
Cyg X-1	2^{16}	57.437	0.059	0.30
Cyg X-3	2^{13}	5.860	0.078	0.20
GX 5-1	2^{16}	22.724	0.044	0.84
GX 1+4	2^{16}	14.76	0.050	1.80

For GX 1+4, the 90% confidence limit amplitude as fraction of source flux exceeds 1.0 indicating that FFT is of no avail to detect any period in the source.

Epoch folding was done on all the data on GX 1+4 (5340s of "on source" time between 10:37 and 13:37 IST) for 40 periods between 94.2 and 98.2s and for 40 periods between 186 and 198s. A maximum χ^2 of 16.03 (for 8 bins) was found for the period of 96.2s. A fit of theoretical χ^2 vs. period to the observed relation /5/ gave a best-fit period 95.9 (0.12)s and amplitude a = 0.015(0.0025), where the 90% error is given in brackets. A maximum χ^2 of 14.33 was found for the period of 191.7s. A fit of theoretical χ^2 vs. period to the observed relation gave a best-fit period 191.7 (0.7)s and amplitude a = 0.010(0.004). The light curve at 95.9s and 191.7s are plotted in Fig. 3, 4 with $\pm 1\sigma$ errors plotted as small circles. We cannot determine whether the shorter or longer period is the neutron star rotation period, however the shorter (96s) period has greater statistical significance.

DISCUSSION AND CONCLUSIONS

Sco X-1 and Cyg X-1 are known to be highly variable in low energy as well as high energy X-rays. The measured temperature and the optically thin plasma of Sco X-1 (E_o = kT = 6.5 ± 0.9 keV) is within the range of variability seen /6/. Cyg X-1 shows a complex time variability, and at least two modes, called the high and low state (see e.g. /7/). As noted in several earlier observations, the spectrum begins to steepen (from a power-law spectrum) in 50-100 keV (Fig. 1). Steinle et al /8/ have hard X-ray balloon data of high statistical accuracy from Cyg X-1 (Sept. 21, 1977) when it was in a low state. Their results are best fit by a Comptonized black-body spectrum with A = 7.4 x 10^{-4}, E_o = 29.2 keV and τ = 5.1 (sphere). Comparing with our model parameters (Table 2) we note that while the temperature and Thompson optical depths are comparable in the two spectra, the absolute flux in the present experiment (1984) is about 0.4 times the 1977 fluxes. Further, our results (Fig. 1) seem to indicate a decline in flux above 100 keV steeper than the best-fit Comptonized spectrum.

The X-ray binary pulsar GX 1+4, is one of the brightest known hard X-ray sources, but was in a low state. The last reported pulsar period measurements were in 1979 and based on the period history in 1974-79, Elsner et al /9/ deduced a period derivative P = -2.681 ± 0.096 s/y. The present period (95.9s) nearly six years after the last measurement gives a P = -2.919 ± .022 s/y. The observed amplitude indicates that nearly 50% of X-rays from GX 1+4 in 18-60 keV are pulsed.

ACKNOWLEDGEMENTS

D.A. Leahy and D. Venkatesan acknowledge support from the Natural Sciences and Engineering Research Council and acknowledge the Space Research Facilities Board/National Research Council (Space Division/NRC, Ottawa) for support in the form of balloons. We wish to thank the following: A.T. Kothare, J.P. Malkar and J.G. Devdhekar for building the payload and instrumentation, A.V. John for help in computation and the staff of the Balloon Facility, Hyderabad for the successful balloon launch. We wish to acknowledge useful discussions with Dr. D. Narasimha.

REFERENCES

1. Damle, S.V., Kothare, A.T., Kunte, P., Malkar, J.P., Naranan, S., Sreekantan, B.V., Venkatesan, D. "A High Sensitivity Phoswich Scintillator X-Ray Telescope for Hard X-Ray (20-120 keV) Astronomy from Balloon Platform" 1986, Proceedings of XXVI COSPAR 86, Toulouse June 30-July 11, 1986.

2. Syunyaev, R.A. and Titarchuk, L.G. "Comptonization of X-rays in Plasma Clouds": 1980, Astron. Astrophys. 86, 121.

3. Damle, S.V., Kunte, P.K., Naranan, S., Sreekantan, B.V., and Venkatesan, D.V. "Hard X-ray Observations of the Quasar 3C273": To appear in Astron. Astrophys. Letters (1987).

4. Leahy, D.A., Darbro, W., Elsner, R.F., Weisskopf, M.C., Sutherland, P.G., Kahn, S., Grindlay, J.E. "On Searches for Pulsed Emission with Application to Four Globular Cluster X-ray Sources: NGC 1951, 6641, 6624, and 6712" 1983, Ap. J. 266, 160.

5. Leahy, D.A. "On Searches for Pulsed Emission: Improved Determination of Period and Amplitude from Epoch Folding for Sinusoidal Signals" 1987, Astron. Ap., 180, 275.

6. Soong, Y. and Rothschild, E. "Long-term, Hard X-ray Observations of Sco X-1 from HEAO-1": 1983, Astrophys. J., 274, 327.

7. Liang, E.P. and Nolan, P.L. "Cygnus X-1 revisited": 1984, Space Science Reviews, 38, 353.

8. Steinle, H., Voges, W., Pietsch, W., Reppin, C., Trumper, J., Kendziora, E., and Staubert, R. "The Hard X-ray Spectrum of Cygnus X-1": 1982, Astron. Astrophys., 107, 350.

9. Elsner, R.F., Weisskopf, M.C., Apparao, K.M.V., Darbro, W., Ramsey, B.D., Williams, A.C., Grindlay, J.E., and Sutherland, P.G. "X-ray Observations of GX 1+4 with the Monitor Proportional Counter on Board the EINSTEIN Observatory". 1985, The Astrophys. J., 297, 288.

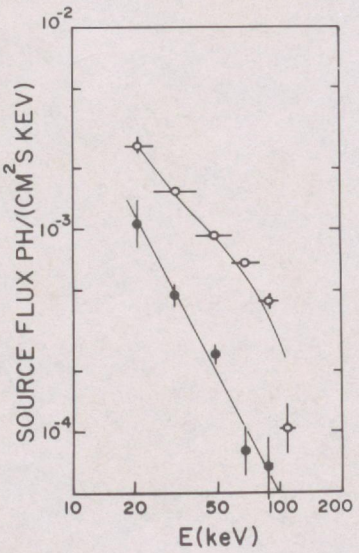

Figure 1.

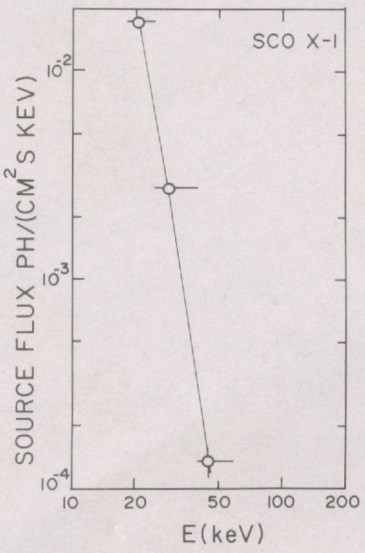

Figure 2.

Adv. Space Res. Vol. 7, No. 7, pp. (7)115–(7)119, 1987
Printed in Great Britain.

0273–1177/87 $0.00+.50

A HIGH SENSITIVITY PHOSWICH SCINTILLATOR X-RAY TELESCOPE FOR HARD X-RAY (20 – 120 keV) ASTRONOMY FROM BALLOON PLATFORM

S. V. Damle,* A. T. Kothare,* P. K. Kunte,* J. P. Malkar,*
S. Naranan,* B. V. Sreekantan* and D. Venkatesan**

**Tata Institute of Fundamental Research, Bombay, India*
***The University of Calgary, Calgary, Alberta T2N IN4, Canada*

ABSTRACT

A large area (400 cm^2) low background X-ray telescope consisting of four collimated NaI/CsI scintillator phoswich detectors (each 100 cm^2) was built and successfully flown several times during 1980-84. The phoswich configuration enables one to eliminate X-ray background produced by high energy atmospheric and cosmic gamma-rays. Combined with large area, small field of view (5° x 5°) and large exposure time that was possible due to an on-board telescope pointing programmer, for the 20 - 120 Kev energy range, 3σ sensitivity achieved was 5×10^{-6} photon/cm^2 sec Kev for exposure time of 10^4 sec at observational altitude of 4 g/cm^2. The Instrument characteristics, relevant details on pointing system, detector system, associated electronics and telemetry and in-flight performance in 1983 and 1984 are presented.

INTRODUCTION

From the UHURU to the Einstein observatory, low energy X-ray astronomy (< 20 KeV) has made great progress; and particularly after the high sensitivity and imaging capability of the latter, soft X-ray astronomy has become fairly competitive to optical and radio astronomies. Such a spectacular growth has not taken place in the hard X-ray (20 - 120 KeV) astronomy, primarily due to intrisic low fluxes involved at these energies and the low sensitivity of the instruments launched thus far on satellites. However, available results (e.g. Cyclotron line at about 60 KeV from Her X-1, energy spectra of QSO's and Seyfert galaxies at > 20 KeV energies) suggest that a wide variety of astrophysical phenomena can best be understood with high sensitivity observations in hard X-rays. This has motivated us in developing a large area low background NaI/CsI phoswichs scintillator detector system for a balloon borne X-ray telescope - TICAL with a possibility, albeit distant, of flying similar system on an Indian satellite. This paper describes the salient features of this telescope and its performance in the balloon flights carried out from Hyderabad (Rigidity cut-off. R ~ 16.8 GV)

THE X-RAY TELESCOPE - TICAL

In a background limited detector system it is well-known that the minimum detectable flux, F_{min}, at 3σ sensitivity is given by $F_{min} = 3/\eta\,(B/A \cdot T \cdot \Delta E)^{1/2}$ ph/cm^2 sec KeV, where η is the efficiency of detection, B is the background in ph/cm^2 sec KeV; A is the area of the detector in cm^2; T is the exposure time in seconds and ΔE is the energy band width in Kev. Therefore, to improve the sensitivity, it is necessary to decrease B, and increase both A and T.

The X-ray telescope - TICAL, consists of four NaI/CsI phoswich scintillator (each 100 cm^2) collimated to 5° x 5° and mounted on an altazimuth programmeable orientation platform with celestial source tracking capability. We briefly describe below, various sub-systems of the TICAL telescope.

The NaI/CsI Phoswich Detector System

Through various early studies /1, 2, 3, 4, 5, 6 / with NaI (Tl) scintillator hard (20 - 120 Kev) X-ray telescopes flown on balloon flights,it has been established that the main source of background is from the Compton interactions of higher energy photons in the thin scintillation detector, producing an energy loss (due to scattered electron) in the relevant X-ray energy band (20 - 120 KeV) To reduce this background, two approaches have been followed by various investigators (a) a back to back version of thin NaI(Tl) main detector and thick NaI(Tl) anti-coincidence detector each seen by different photomultipliers (PMs) /7/ and (b) a composite phoswich scintillator with NaI(Tl) and CsI(Tl) or CsI(Na) as anti-coincidence detector, viewed together by the same PM tube /8, 9/. As

NaI(Tl) and CsI(Tl) or CsI(Na) scintillations have different fluroescent decay constants, a pulse shape discrimination (PSD) technique allows selection of X-ray events only from the main thin NaI(Tl) X-ray detector. We have used a 3 mm thick NaI(Tl) and 25 mm thick CsI(Na) phoswich scintillator system, 125 mm in diameter viewed by an EMI 9530 PM tube as the basic X-ray detector. The fluorescent decay time constant of 0.23 μsec for NaI(Tl) and 0.63 μsec for CsI(Na) are sufficiently different to separate the events originating in the two scintillators.

Fig 1. shows one of the four similar NaI(Tl)/CsI(Na) phoswich scintillator detector PM tube assembly with 5° x 5° square collimator enclosed inside a graded shield (3 mm lead, 3 mm tin and 1 mm copper) and the Pulse Shape Discrimination (PSD) circuit scheme. The effective area of the detector is 100 cm^2 ; and four detectors together provide a total detector area of 400 cm^2.

In the phoswich detector, three types of events are seen: (1) NaI(Tl) only - these are mainly due to X-ray events (2) CsI(Na) only - these are due to background photons from backward direction and from the sides; (3) NaI(Tl) (+) CsI(Na) events - these are mainly due to Compton scattered events in the NaI(Tl). We accept only those events which show energy loss in the range 18 - 120 KeV (pulse height - PH) in the detector assembly. Further, to select only type 1 NaI(Tl) events, we subject the PH selected events for a pulse shape (PS) analysis. This is achieved by using a new pulse shape discrimination circuit (PSD) circuit specifically developed for this experiment /10/. The principle of the PSD scheme which separates events of type 1 from type 2 and 3 is based on the comparison of the peak of anode pulse with a fixed proportion of its own peak amplitude. The PSD circuit generates a gate whose width is proportional to the decay time of the anode pulse i.e. pulse shape (PS). The PS and PH information for each selected event is digitised by using an onboard 127 channel analyser and fed to the telemetry encoder, along with the event time information (accurate to 40 μ sec).

A well-collimated Am^{241} radioactive source mounted above the collimator and preprogrammed to periodically shine over each detector for 20 seconds in a specific sequence, provides in-flight calibration for PH and PS for each detector. A cradle structure, free to rotate in a preprogrammed mode on its horizontal axis (Elevation axis) houses the entire detector assembly.

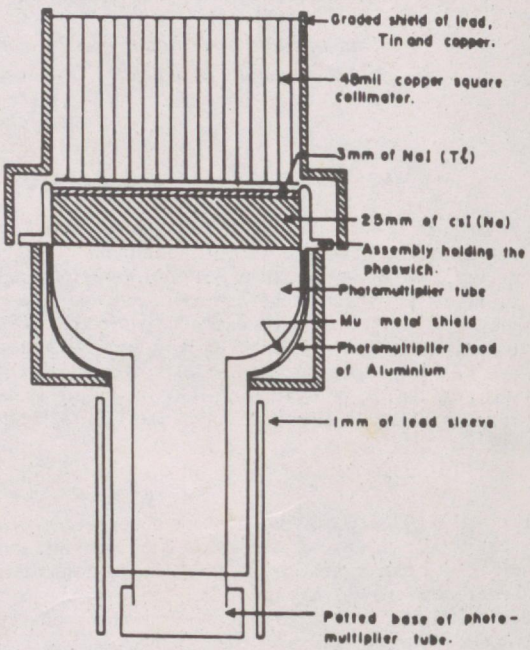

Fig 1. NaI(Tl)/CsI(Na) Phoswich Detector and Photomultiplier Assembly with Collimator (5° x 5°) And Graded Shield Assembly.

The Pointing System, Electronics and Telemetry

The X-ray telescope is an alta-azimuth mounted system and has a programmed control for pointing in azimuth and elevation; it is schematically shown in Fig 2. An integrated assembly of detectors and electronic hardware is mounted on a servo-controlled main azimuth platform. The azimuth pointing employs a null-seeking servo system in which a reaction wheel control is used and the flux gate magnetometer (FGM), M1 provides position sensing in the azimuth. Any deviation from the null (East-West direction) due to balloon perturbations, provides an output from M1 through servo amplifier to the torque motor, to regain the null position. The capability to track in the azimuth and elevation is achieved by following scheme. M1 is mounted on a turn-table driven by a stepper motor; a shaft encoder (SE1) provides instantenous position of M1 and hence the telescope azimuth. A geared servo motor provides a controlled drive for the elevation axis coupled to a shaft encoder (SE2) which provides the instantenous elevation aspect. An additional azimuth aspect is provided by a set of crossed FGM's M2 and M3. Thus SE1 and SE2 together withn M2 and M3 provide complete aspect information for the X-ray telescope. The entire system is calibrated on ground with respect to the star Polaris. The rms pointing accuracy achieved is 0.35 degrees in azimuth and elevation. During a balloon flight, the elevation control motor and the stepper motor of the turntable with M1 could be driven through remote control or through commands generated by an onboard position control programmer (PCP). This scheme facilitates a programmed observation of celestial X-ray sources and corresponding background by tracking in azimuth and elevation during a balloon flight.

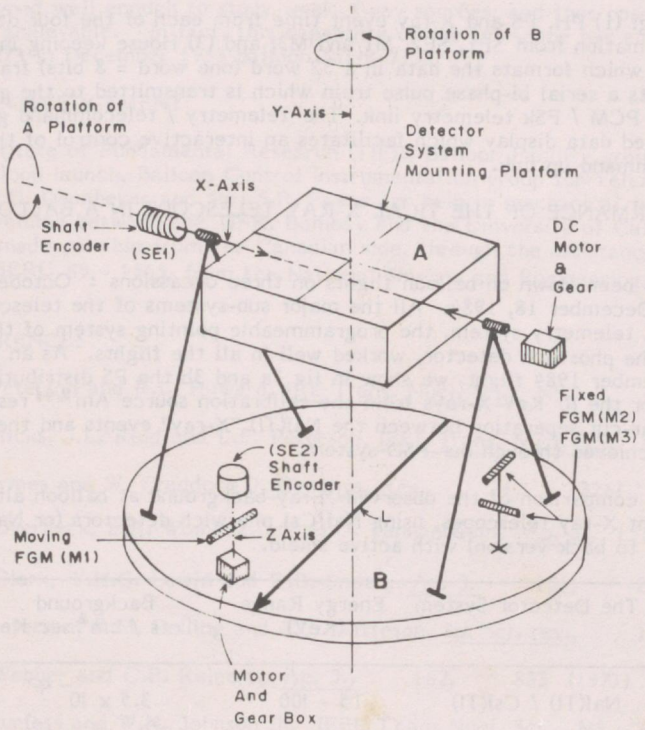

Fig 2. A Schematic of the X-ray Telescope (TICAL)

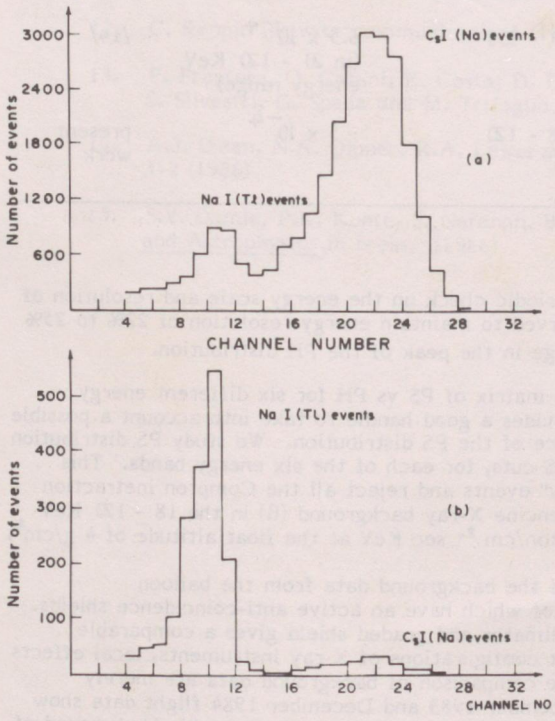

Fig 3. The PS Distribution, Observed in the December, 1984 Balloon Flight:(a) For Background Events And (b) For the Am X-ray Events

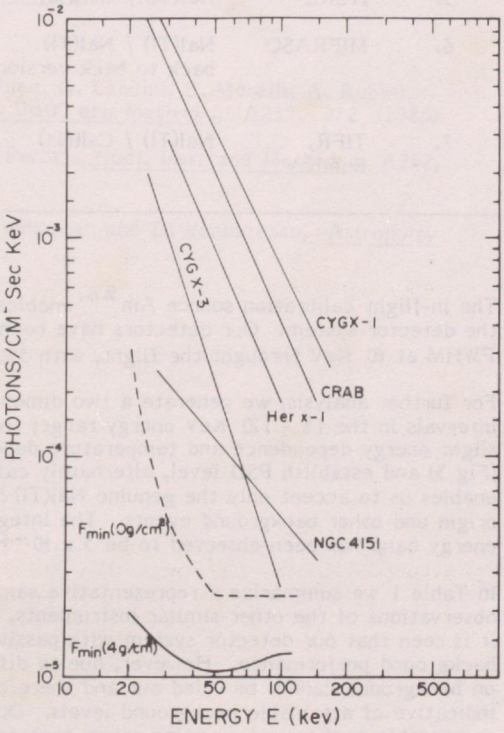

Fig 4. The 3σ sensitivity of the X-ray Telescope

The basic data comprising: (1) PH, PS and X-ray event time from each of the four detectors; (2) telescope aspect information from SE1, SE2, M1 and M3; and (3) House keeping information, is fed to a PCM encoder which formats the data in a 32 word (one word = 8 bits) frame (128 frame = 1 sub-frame) and outputs a serial bi-phase pulse train which is transmitted to the ground station through a 50 kbits/sec PCM / FSk telemetry link. The telemetry / telecommand ground station provides an on-line decoded data display which facilitates an interactive control of the X-ray telescope through telecommand up link.

THE PERFORMANCE OF THE TICAL X-RAY TELESCOPE IN A BALLOON FLIGHT

The TICAL telescope has been flown on balloon flights on three occassions : October 30, 1980; December 12, 1983 and December 18, 1984. All the major sub-systems of the telescope --- the 50 k bits/sec PCM / FSK telemetry system, the programmeable pointing system of the telescope and the PSD system of the phoswich detector, worked well in all the flights. As an illustration, based on data from December 1984 flight, we show in fig 3a and 3b the PS distribution for the background events and for the 60 KeV X-rays from the calibration source Am^{241} respectively. It is observed that a clear-cut separation between the NaI(Tl) "X-ray" events and the CsI(Na) "background" events is achieved through our PSD system.

TABLE 1. A comparison of the observed X-ray background at balloon altitudes with different X-ray telescopes, using NaI/CsI phoswich detectors (or NaI(Tl)/ NaI(Tl) back to back version) with active shield.

Sr. No.	Group	The Detector System	Energy Range (KeV)	Background cts / cm^2 sec KeV	Reference
1.	UCSD	NaI(Tl) / CsI(Tl)	15 - 100	3.5×10^{-4}	/8/
2.	NRL	NaI(Tl) / CsI(Na)	30 - 100	2.5×10^{-4}	/7/
3.	MPI/ATI	NaI(Tl) / CsI(Tl)	20 - 130	4.8×10^{-4}	/11/
4.	MPI/ATI	NaI(Tl) / CsI(Tl)	20 - 120	3.3×10^{-4}	/12/
5.	ITSRE	NaI(Tl) / CsI(Na)	20 - 120	2.5×10^{-4}	/13/
6.	MIFRASO	NaI(Tl) / NaI(Tl) back to back version	20 - 300	6.5×10^{-4} (in 20 - 120 KeV energy range)	/14/
7.	TIFR, Bombay	NaI(Tl) / CsI(Na)	18 - 120	5×10^{-4}	present work

The in-flight calibration source Am^{241} enables a periodic check on the energy scale and resolution of the detector system. Our detectors have been observed to maintain energy resolution of 22% to 25% FWHM at 60 KeV throught the flight, with 5% change in the peak of the PH distribution.

For further analysis, we generate a two dimensional matrix of PS vs PH for six different energy intervals in the 18 - 120 KeV energy range; this provides a good handle to take into account a possible slight energy dependence and temperature dependence of the PS distribution. We study PS distribution (Fig 3) and establish PSD level, alternately called PS cuts, for each of the six energy bands. This enables us to accept only the genuine NaI(Tl) "X-ray" events and reject all the Compton inetraction origin and other background events. The integral genuine X-ray background (B) in the 18 - 120 KeV energy band has been observed to be 5×10^{-4} photon/cm^2 sec KeV at the float altitude of 4 g/cm^2.

In Table 1 we summarize a representative sample of the background data from the balloon observations of the other similar instruments, most of which have an active anti-coincidence shields. It is seen that our detector system with passive collimator and graded shield gives a comparable background performance. However, due to different configurations of X-ray instruments, local effects on background cannot be ruled out and therefore the comparison of background data are merely indicative of attainable background levels. Our December 1983 and December 1984 flight data show comparable background counting rates, thus confirming the genuine nature of the stable background of our instrument. Assuming a background limited celestial X-ray source detection, we calculate the 3σ sensitivity of the X-ray telescope for the area A = 400 cm^2 of our system and typical exposure time $T = 10^4$ sec equal for source and background. In fig. 4 we show the 3σ sensitivity at float altitude (4 g/cm^2); and the one referred to the float altitude (0 g/cm^2) and the differential

X-ray spectra of some of the Cosmic X-ray sources. It is observed that the sensitivity of our instrument is designed well enough to study weak X-ray sources, and thus observation of AGN's amongst others is achievable. In fact, this capability of the telescope has enabled us to observe the nearby quasar 3C273 in December 1983 balloon flight /15/.

ACKNOWLEDGEMENT

We thank Tata Institute of Fundamental Research (TIFR) Balloon Facility group, Hyderabad, for conducting the balloon launch, Balloon Control Instrumentation group for Telemetry, Telecommand Support and Shri J.G. Deodhekar and Shri S.P. Pawar for help in mechanical fabrication. The collaboration programme between the TIFR, Bombay and the University of Calgary, Calgary, Alberta, Canada, has been made possible from the Canadian side, through the assistance to D. Venkatesan, under the grant NSERC 69 - 1565, from the National Science and Engineering Research Council, Ottawa, Canada.

REFERENCES

1. L.E. Peterson and R.L. Howard, IRE Trans. Nucl. Sci., NS - 8, 21 (1961)

2. D.B. Hicks, J.L. Reid and L.E. Peterson, IEEE Trans. Nucl. Sci., NS - 12, 54 (1965)

3. R. Haymes and W. Craddock J. Geophys. Res., 71, 3261, (1966)

4. J.W. Overbeck, E.A. Womack, and H.D. Tannanbaum, Ap. J., 151, 21, (1967)

5. G.W. Clark, W.H.G. Lewin and W.B. Smith, Ap. J. 151, 21 (1968)

6. L.E. Peterson, R.M. Pelling and J.L. Matteson. Sp. Sci. rev., 13, 320 (1972)

7. W.R. Webber and C.P. Reinert, Ap. J., 162, 883 (1970)

8. J.D. Kurfess and W.N. Johnson III. IEEE Trans,Nucl. Sci., NS - 22, 626 (1975)

9. J.L. Matteson, P.L. Nolan, W.S. Paciesas and R.M. Pelling, Sp. Sci. Rev., 3, 491 (1977)

10. J.P. Malkar and P.K. Kunte, Nucl. Instr. and Methods., 202, 465 (1982)

11. C. Reppin, W. Pietsch, J. Trumper, W. Voges, E. Kendziorra and R. Staubert, Proc. Esrange Symposium, Ajaccio, (ECA SP - 135), 293, (1978)

12. C. Reppin (private communication) (1982)

13. F. Frontera, O. Catani, E. Costa, D. Dal Fiume, G. Landini, E. Morelli, A. Rubini, S. Silvestri, G. Spada and M. Trifoglio, Nucl. Instr. and Methods., A235, 372 (1985)

14. A.J. Dean, N.A. Dipper, R.A. Lewis and F. Perotti, Nucl. Instr and Methods., A242, 342 (1986)

15. S.V. Damle, P.K. Kunte, S. Naranan, B.V. Sreekantan and D. Venkatesan, Astronomy and Astrophysics, in press, (1986)

(BAKSAN 87)
UP-87

RESULTS ON MONOPOLES AND KOLAR EVENTS FROM KGF EXPERIMENTS

H. Adarkar, M.R. Krishnaswamy, M.G.K. Menon, N.K. Mondal,
V.S. Narasimham, B.V. Sreekantan
Tata Institute of Fundamental Research, INDIA

Y. Hayashi, N. Ito, S. Kawakami, T. Nakamura
Osaka City University, JAPAN

S. Miyake
Kanegawa University, JAPAN

Abstract

In this paper we present the status of the search for monopole signals as well as the Kolar events with the deep underground experiments being conducted in the Kolar gold mines. The proton decay detectors at the depths of 2 and 2.3 km have dE/dX as well as time of flight capabilities. In view of the absence of candidate events we could set an upper limit to the flux of monopoles as $4 \times 10^{-15}/cm^2.sec.st$. Two examples of Kolar events are presented here; these are indicative of the production of hitherto unknown particles of mass >2 GeV and life time $10^{-9} - 10^{-8}$ sec in processes akin to neutrino interactions.

1. Introduction. The KGF experiment consists of two detectors (Phase I & II) at the depths of 7000 and 6045 hg/cm^2. They are designed primarily as fine-grain calorimeters to search for proton decay signals. A detailed description of the detectors, the trigger features etc. was given earlier /1/. Briefly, they comprise horizontal layers of proportional counters (filled with P10 gas) and arranged in an orthogonal array. The individual counters are formed from 2.3 mm thick iron tubes and they account for a substantial portion of the weight of the detector; the horizontal layers are interspersed with thin iron plates to provide additional absorber. Various features of these detectors are given in Table 1. The primary trigger is obtained from a coincidence pulse in at least 5 out of 11 consecutive layers; large angle events are selected by a special 2-fold coincidence trigger. To search for monopoles, the coincidence window is expanded to 7 and 18 μ sec with a minimum number of layers of 7 and 8 respectively for Phase I and II detectors.

A new design feature of the Phase II detector is the outer jacket separated from the main array by 1-1.5 m to enhance the fiducial weight for nucleon decay events as well as to examine the Kolar-type events in greater detail. The jacket is, at present, on three sides only and comprises two walls of counters and two 1" thick absorbers per side.

Each counter is instrumented to record the ionisation as well as the time of arrival information with resolution as given in Table 1. The ionisation data is obtained in terms of the number of minimum ionising particles traversing a counter in the vertical direction. As the detectors are operated deep underground, the event rate is very small and a major fraction of them are due to atmospheric muons; events with zenith angles $\geq 60°$ are primarily due to neutrino interactions in the rock giving rise to muons. In addition to these, there are events due to ν-interaction inside the detector itself which constitute the main background for nucleon decay candidates.

Table 1

Experimental details	Phase I	Phase II
Depth	2.3 km (7000 hg/cm²)	2.0 km (6045 hg/cm²)
Size	6m x 4m x 3.6m	6m x 6m x 6.5m
# layers (counters)	34 (1594)	60 (3836)
Absorber (Fe)/layer	12mm	6mm
Total (Fid.) weight	140 (60) tons	350 (150) tons
Threshold	1/4 I_{min}	1/4 I_{min}
Timing resolution	500 nsec	200 nsec
Mean density (gm/cm³)	1.7	1.1
S Ω for > 1.5m path for isotropic radiation	270 m² st.	570 m² st.
Live time (Years)	5.14	1.1
# atmospheric muons	3710	3666
# ν-induced events from rock	88	44
#confined events	26	8

2. Massive monopoles. Two methods were employed to search for GUT monopoles in the detector: (i) Ionisation and (ii) time of flight.

(i) Ionisation: In this method advantage is taken of the measurement of the energy loss over a large dynamic range of pulse height and many samplings along the length of a track. The search was confined to tracks with path length >1.5m to have at least 12 samplings and for particles with mean ionisation >2.5 I_{min} so as to suppress effects of the tail of the single particle distribution and eliminate ≧ 2 closely spaced parallel muons, from the sample. The cut on ionisation restricts the monopole search to velocities > 1.4 x 10^{-3}c. A statistical analysis of the data for uniform ionisation at any value >2.5 I_{min} within the resolution ($\sigma = 0.25/\sqrt{N_{eq}}$,

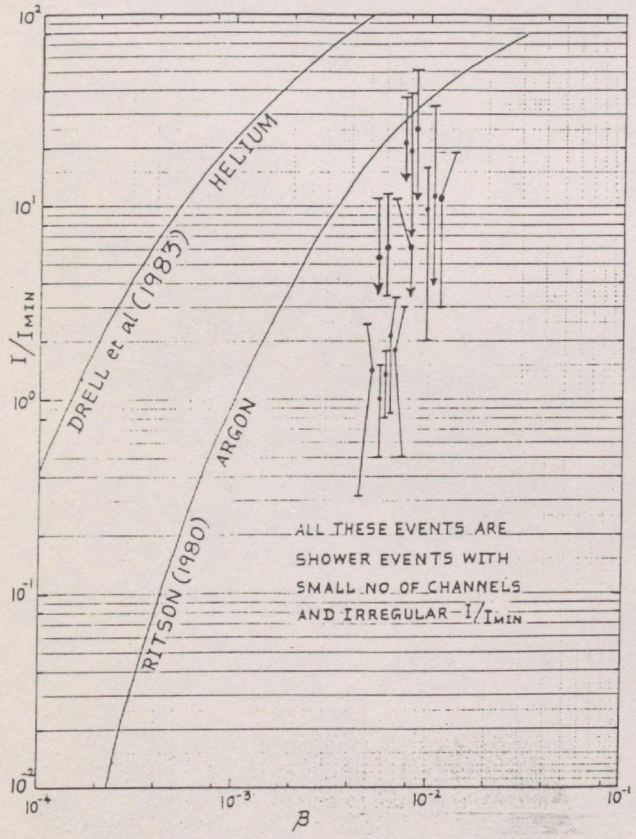

Fig. 1. A plot of I/I_{min} against lowest possible β obtained through a χ^2 test. The events shown have high ionisation inconsistent with their low velocity. However, all these events are showers and have non-uniform ionisation.

$N_{eq} = I/I_{min}$) has failed to identify even a single candidate. Combining the exposures of the two detectors, the upper limit on the flux of monopoles at 90% confidence level is 2.3/6.0 x 10^{14} = 3.9 x 10^{-15}/cm².sec.st.

(ii) Time of flight method: Both the detectors are sensitive to slow moving monopoles in the velocity region 7.5×10^{-4}C - 5×10^{-3}C, the lower value arising from the trigger threshold and the upper from the timing resolution. For the Phase II detector, however, the upper cut-off is 1.2×10^{-2}C due to 200 nsec resolution of its timing circuits. All events with pathlength > 1.5 m were searched for slow moving monopoles by analysing the timing data in terms of minimum velocity to which they can be fitted, consistent with the resolution function. All the events have velocities > 5×10^{-3} C and only a few of them can be fitted to velocity < 1.2×10^{-2} C (Fig. 1). The later sample was examined in detail and was found to comprise events of non-uniform shower profile, inconsistent with the expected character of a monopole signal. The upper limit to the flux of monopoles at 90% C.L is then $2.3/5.6 \times 10^{14} = 4.1 \times 10^{-15}/cm^2.sec.st.$ for $7.5 \times 10^{-4} < \beta < 5 \times 10^{-3}$.

3. Kolar events. We have recorded a special event (Fig. 2) in Phase II detector with the following general features. There are two sets of tracks in the event of which one is a penetrating track 'A' and the other a shower 'B'; the meeting point 'P' of these tracks is outside the detector (in air), 30 cm away from the side of the detector in the airgap and ∿ 7 m away from the rockwall in the direction of the event. The uncertainties due to the shower pattern can bring the vertex nearer to the detector by ≦ 10 cm but still clearly in the air. Yet another event recorded in Phase I unit has the same general features but its vertex could have been either in air or rockwall (Fig. 3). The characteristic features of these two events are summarised in Table 2.

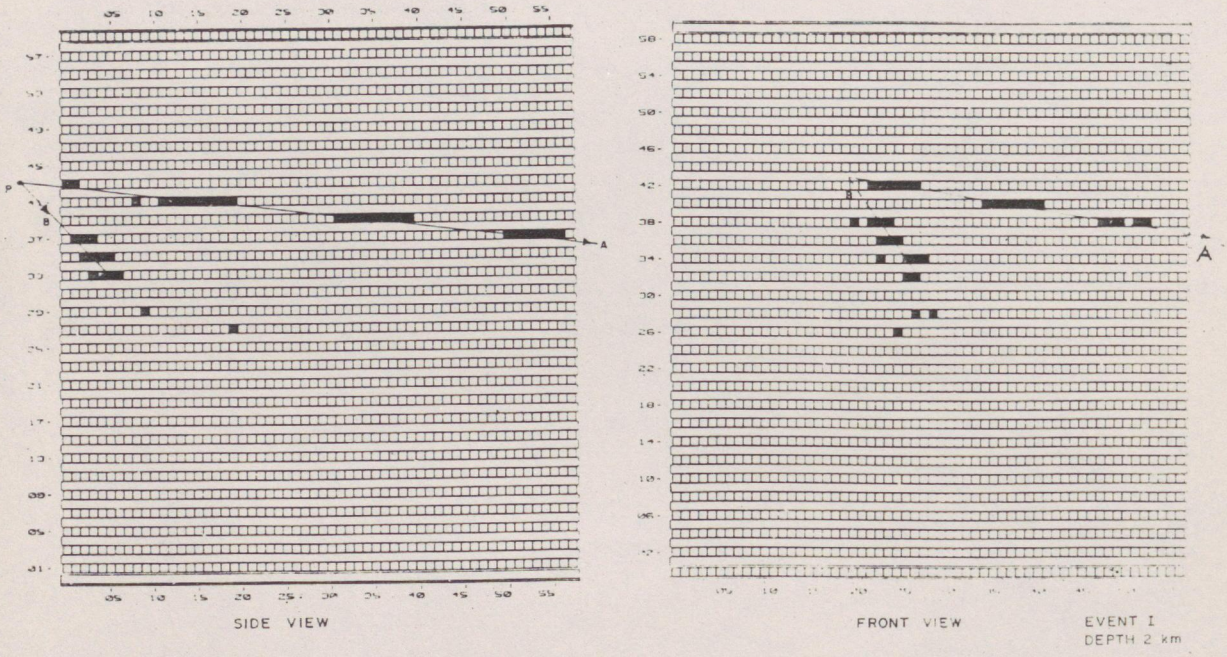

Fig. 2. The two orthogonal views of Kolar Event 1 recorded at the depth of 2000 m in Phase II detector. Track A is a penetrating muon with a zenith angle of 85° and track B is a fully absorbed shower at a mean zenith angle of 53°. The meeting point P of these two tracks is about 30 cm away from the detector and ∿ 7 m away from the nearest rock wall.

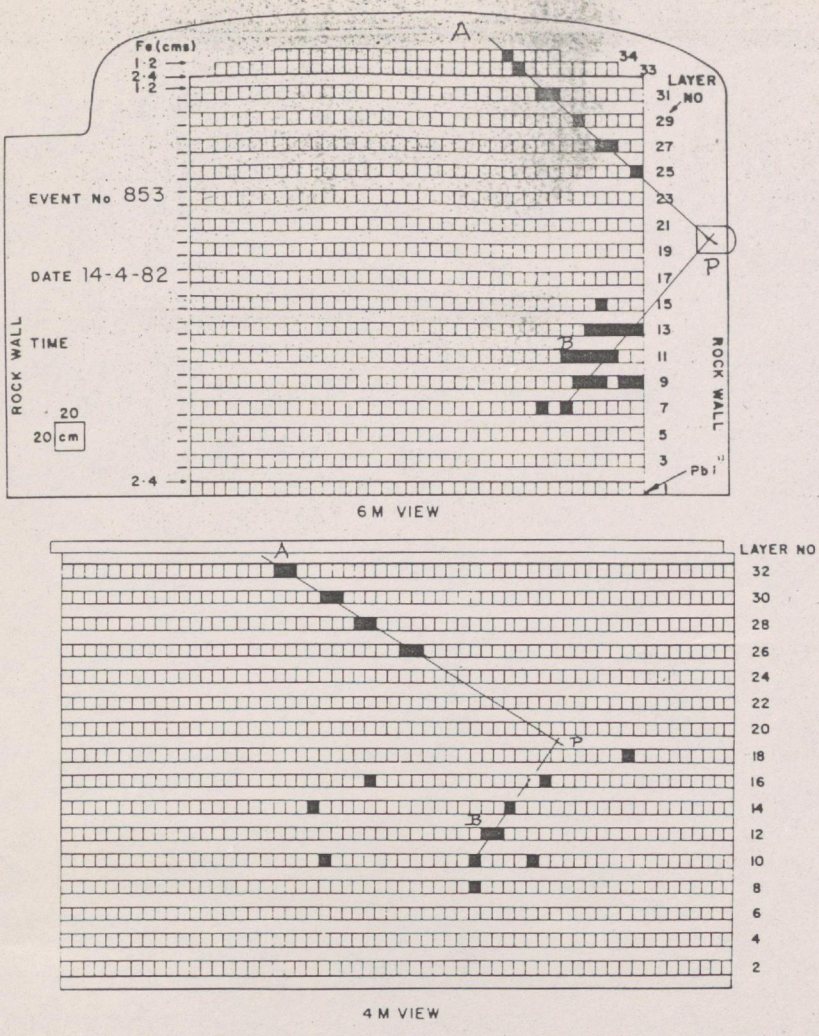

Fig. 3. A sketch of Kolar Event 2 recorded in Phase I detector at the depth of 2300 m. Track A has a zenith angle of 62° (upward) and track B, a shower, has a zenith angle of 51° (downward). The vertex P of these two tracks could be in air or inside rock with equal probability due to the uncertainty in the angle of the shower B.

Table 2

	Event 1	Event 2
Detector	Phase II	Phase I
Depth	2.0 km	2.3 km
Vertex	in air	in air or rock
Opening angle	32 ± 5°	69 ± 5°
$E_{\text{penetrating track}}$	>1.3 GeV (Range 900 gm/cm²)	>0.45 GeV
E_{shower}	>2.6 GeV	>2.5 GeV

The opening angles of the two tracks from the reconstructed vertex is large in both these events. Also since the ionisation is recorded for each channel, the energy of the showers is estimated by the track length integral method from the ionisation data. For the energy of the penetrating tracks however, we have set lower limits by the range-energy method assuming the particle

to be a muon. It should be pointed out that in both these events, the mean incident direction is near horizontal and the total visible energy is 3-4 GeV.

We consider these two events as belonging to a special class called 'Kolar Events'. Ordinary backgrounds like bremmstrahlung of a muon or the decay of K_L^o produced in muon or neutrino interactions are ruled out because of (i) the large opening angle of the tracks at the vertex and (ii) the minimum energy (2.5 GeV) of the shower. The fact that the vertex is in air (event 1) and the large opening angle (>32°) indicates that a decay of a particle of mass > 2 GeV/c^2 is involved here. Further, since at least in the case of event 1, the vertex is $\geq$ 7 m away from rock a lifetime of 10^{-9} to 10^{-8} sec. is indicated if we assume that the present particle was produced in the fringes of the rockwall.

4. Conclusions. The two nucleon decay detectors Phase I and Phase II have not so far recorded any possible massive monopole candidate; this indicates an upper limit of their flux of 4.1 x 10^{-15}/cm^2.sec.st. in the velocity region 7.5 x $10^{-4} < \beta < 1$. A 19-layer detector of 36 m^2 area is under construction by the side of Phase II detector. The 8 middle layers of this new unit will have counters filled with 83% He + 17% CH_4 mixture to reduce the velocity threshold down to 3 x 10^{-4}c using Drell mechanism.

Two examples of 'Kolar Events' have been recorded, one in each detector, indicating the decay of hitherto unknown particle of mass > 2 GeV/c^2 and lifetime of 10^{-9} - 10^{-8} sec. We need more events of this type especially in fine-grain detectors to pin point their nature and origin more clearly.

5. Acknowledgements. We are grateful to the Bharat Gold Mines Ltd. for the facilities provided. Messrs. S.R. Dugad, B. Satyanarayana, S. Kalmani, P.S.N. Murthy and T. Nagaraj helped in assembly and maintenance of the detector and we thank them. Finally we thank the Japanese Council for Promotion of Science for partial financial help.

References

1. Krishnaswamy M.R. et al.//Proc. XXIII Int. Conf. on High Energy Physics, Berkeley, U.S.A., 1986, Vol. 2, P. 1290.

Astron. Astrophys. 178, 242–246 (1987)

ASTRONOMY
AND
ASTROPHYSICS

Very high energy gamma-rays from the Vela pulsar

P.N. Bhat, S.K. Gupta, P.V. Ramana Murthy, B.V. Sreekantan, S.C. Tonwar, and P.R. Vishwanath

Tata Institute of Fundamental Research, Homi Bhabha Road, Bombay 400005, India

Received October 8, accepted December 10, 1986

Summary. PSR 0833-45 was observed by us on several occasions over a time span of 5 yr using the wellknown atmospheric Cerenkov technique. All the available observations with absolute phase information constitute 3 independent data-sets with slightly differing gamma ray energy thresholds in the range 5 to 10 TeV. These data-sets are separately analysed and the phasograms are derived using the pulsar elements derived from radio measurements. Two of the three phasograms show an excess at the same phase bin which coincides with the expected position of the optical first pulse. However, the statistical significance of the signal improves when only the lower energy showers are chosen, based on the pulse height information and/or the source hour-angle. When all the 3 phasograms after applying this cut, are summed, the resultant phasogram shows a 4.0σ peak at the optical phase. There is a hint of a weak second pulse of 1.5σ at phase 0.7. Allowing for various degrees for freedom, one obtains a value of $2.7\ 10^{-5}$, for the probability that all the excesses are statistical fluctuations. From the excesses observed at different gamma ray energy thresholds an integral energy spectrum of the TeV gamma rays from Vela is derived. The estimated slope of this power law energy spectrum is $-(2.5 \pm 0.3)$

Key words: pulsars: PSR 0833-45 – pulsars: Vela pulsar – Gamma rays: very high energy – atmospheric Cerenkov technique

1. Introduction

Discovered in the radio wavelength during late 1968 by the Molonglo group (Large et al., 1968) Vela pulsar is located near the centre of the large supernova remnant Vela X. It is one of the fast pulsars with a period of about 89 ms and its distance is about 500 pc. The emission from this pulsar is similar to that from the wellknown Crab pulsar, at various wavelengths. However there are some marked differences compared to the Crab pulsar. The radio light curve of Vela pulsar shows only one pulse. In the X-ray energy band no significant emission is detected from this pulsar (Knight et al., 1982). Even though both the pulsars show double peak in their light curves in optical and gamma ray bands their phases coincide in the case of Crab pulsar but not in the case of Vela pulsar. The luminosity above 100 MeV for Vela is about 3.6 times that of Crab whereas pulsed emission from Vela at optical wavelengths is less than $2\ 10^{-4}$ of that from Crab (Thompson et al., 1975; Manchester et al., 1978).

Measurements of relative phases of pulsed emissions in radio, optical and medium energy gamma rays show that the radio peak (by definition at phase = 0) is followed by the first gamma ray peak at 11.2 ms, the first optical peak at 21 ms, the second optical peak at 42 ms and finally the second gamma ray peak at 49 ms (Buccheri et al., 1978). This indicates that probably the mechanisms and certainly the sites of production of radiation at radio, optical and gamma ray wavelengths are different. The near coincidence of the midpoints of the optical and gamma ray pulse profiles led Manchester and Lyne (1977) to suggest that both the components are emitted from a single magnetic pole of the neutron star. But the improved data show that the midpoints are no longer quite coincident, being at 30.5 ms and 31.5 ms for optical and gamma ray region respectively (Buccheri et al., 1978).

In the medium energy gamma ray range strong emission showing a clear double pulse structure in the phasogram was detected by SAS-2 as well as COS-B experiments (Thompson et al., 1975 and Bennett et al., 1977). All the emission in this energy range seems to be pulsed, bulk of which is contained in two narrow pulses with FWHM of about 3 and 6 ms respectively, with a characteristic separation of 0.42 in phase. However, what is interesting in the present context, is the structure in the intra-pulse region; specifically an excess is seen at the phase of the first optical pulse. Even though it is only a suggestion in the observed COS-B data, it looks as though the feature persists until the highest COS-B energy range viz: 1.5–3 GeV.

In the very high energy (VHE) range, there have been several observations so far both by our own group as well as by Grindlay et al. (1975). Grindlay et al., detected 4.2σ and 3.0σ peaks in the pulsar phasogram in 1972 and 1973 observations respectively. The same group derived upper limits using their total data of 1973 and 1974 observations (see Grindlay, 1982). We had detected a positive signal from the Vela pulsar on two previous occasions; i.e. prior to the observations discussed here. The phasogram derived from the 1979 observations (while the gamma ray threshold was 10.4 TeV) showed 2 peaks of 4.4σ and 2.5σ respectively separated by 0.42 of phase (Bhat et al., 1980). During 1980–81 (while the gamma ray energy threshold was 7.0 TeV) observations using the distributed array, the data showed a 4.3σ peak in the phasogram (Gupta et al., 1982). On both these occasions there was no information on the absolute pulsar phase. In this paper, we will present the results from our later (1979–85) observations using a compact array; we have absolute phase information in these data.

Send offprint requests to: P.N. Bhat

2. Observations

The observations were carried out at Ootacamund (S. India) which is situated at 11°.4 N latitude and 70°.7 E longitude and at an altitude of 2.2 km above mean sea level. The technique used is the well-known atmospheric Cerenkov technique, which is ideally suited for the study of gamma rays in this energy range (see Porter and Weekes, 1979; Ramana Murthy, 1980). The atmospheric Cerenkov telescope consisted of 18 parabolic reflectors; 8 of them were 1.5 m diameter and the remaining of 0.9 m diameter deployed in a closely packed array. The mirrors were mounted on individual equatorial mounts. The total physical area of the reflectors was 20.5 m^2 (for details see Gupta, 1983). Using this system, even the sources with large declinations (e.g. the Vela with $\delta \sim -45°$) could be tracked for more than 2 hr each before and after the source transit.

The observations on the Vela pulsar were carried out during 1979–80, 1982–83 and 1984–85 in the tracking mode whence the source was continuously tracked for 1–4 hr during each run. We observed Vela for a total of 3943 min in 1979–80, 2147 min during 1982–83 and 1747 min during 1984–85.

During the observations of all the three years the trigger was generated by a nearly identical electronic logic system. The pulses from the photomultipliers mounted at the focus of each mirror are added to form 4 or 6 banks. Pulses from each bank are amplified (gain ~ 10) and fed to fast discriminators. The logical pulses generated by the discriminators (FWHM $\sim$ 15–20 ns) are in turn used to generate the trigger by a majority logic unit. An identical majority logic unit is used wherein the logical inputs are connected after being relatively delayed by various amounts. This unit generates the chance coincidences which are monitored simultaneously during the course of a run. The high voltage on the photomultipliers were adjusted such that the chance coincidence rate was less than $\sim 10\%$ of the total trigger rate.

During the runs in 1982–83 and those in 1984–85, the pulse heights of a bank were digitized using a 11 bit fast ADC and recorded along with the event time and other data on a magnetic tape. Until 1984, we were calibrating our clock by using the atomic time signals broadcast by National Physical Laboratory, Delhi. This was cross checked by a similar calibration done using the time signals from a Chinese broadcasting station. With this procedure we could maintain the accuracy in absolute time of ± 1 ms. In 1984–85 season we used a satelite timing receiver which is capable of correcting itself using the coded time signals received from US Navy satellites (NNSS) once every few hours. The accuracy of this clock is $\pm 30\,\mu$s in absolute time.

3. Analysis and results

The data taken during 1979–80, 1982–83, and 1984–85 form 3 independent data sets. These 3 data sets were analysed separately. The arrival times of each event, after suitably correcting for time calibration whenever necessary, are converted into the corresponding times at the solar system barycentre using a program which uses the MIT barycentric ephemeris (Ash et al., 1967). Then the pulsar phase at this time was deduced using the pulsar elements supplied to us by R.N. Manchester (1979–80), R.W. Royle (1982–83) and A.R. Kleckociuk (1984–85) using radio observations. Thus a 30-bin phasogram of the events is derived for each data set and bins showing significant excess events are searched in each phasogram. The absolute phase with respect to the radio peak is known in each case.

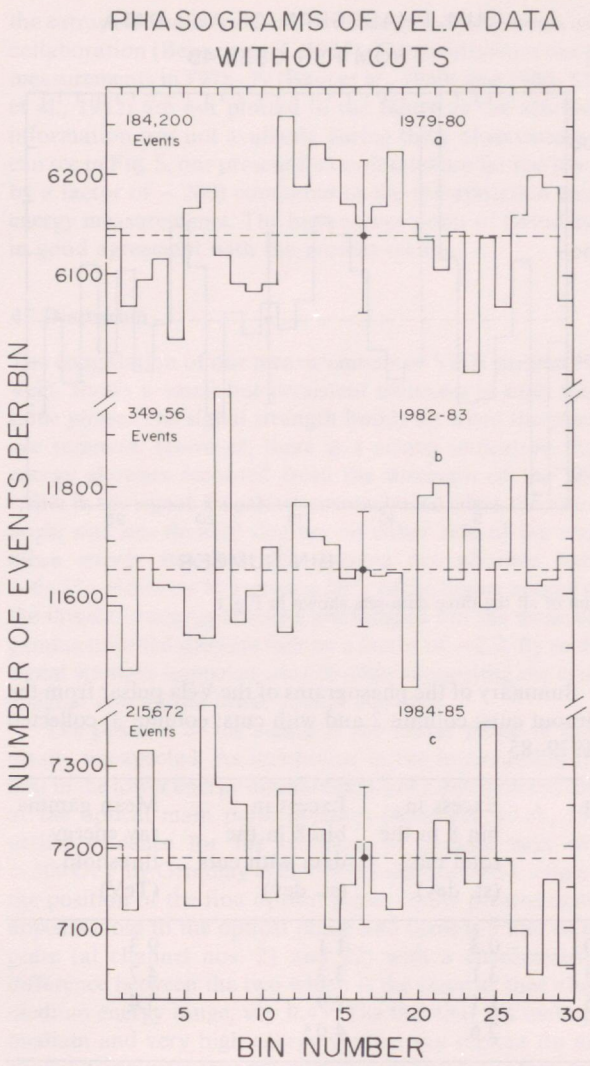

Fig. 1. Phasogram of all the recorded events from the direction of PSR 0833–45 during (a) 1979–80 (b) 1982–83 and (c) 1984–85

Figure 1 shows the phasogram of all the recorded events in each data-set 1979–80, 82–83, and 84–85 with respect to the radio phase. The estimated mean gamma ray energy thresholds for these data sets are respectively 10.4 TeV, 4.9 TeV and 5.8 TeV, averaged over all hour angles of the observation. It is apparent that there is no significant ($\gtrsim 4\sigma$) excess in any of the three phasograms in any phase bin. However, it may be pointed out that there is a small excess in channel number 8 in 2 of the data sets. Even though these excesses are not significant by themselves, their repetition over the years in the same phase bin makes them significant. Figure 2 shows the sum of the all the 3 phasograms with respect to the radio phase. As the excess occurs at the same phase bin the signal in the final phasogram is 2.6σ in bin 8. This phase bin corresponds to absolute pulsar phase of 0.27. However the phase at which the pulse appears is very close to optical first pulse (0.24, Buccheri et al., 1978). Table 1 (column 2) summarizes the relevant numbers derived from Figs. 1 and 2.

Among the 3 phasograms in Fig. 1, (b) has the lowest gamma ray energy threshold viz. 4.9 TeV. Also, this phasogram indicates more prominently (3.1σ and 2σ respectively) the existence of a

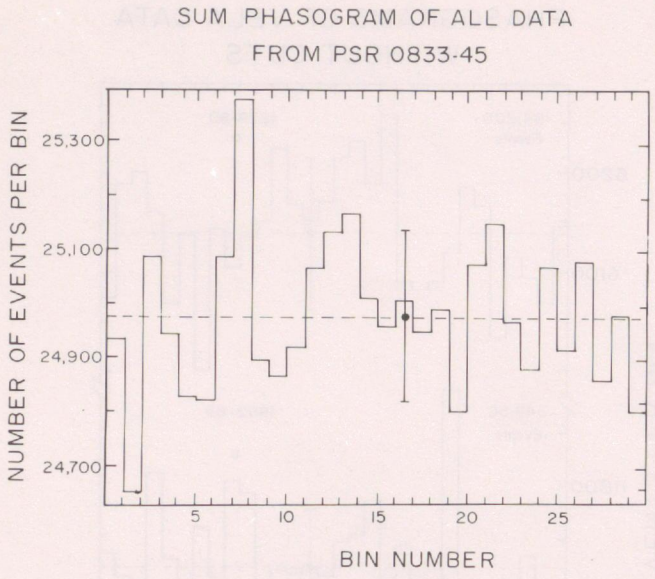

Fig. 2. Sum of all the three data-sets shown in Fig. 1

Table 1. Summary of the phasograms of the Vela pulsar from the data (without cuts: column 2 and with cuts: column 3) collected during 1979–85

Data set	Excess in bin 8 in the total data (st. dev)	Excess in bin 8 in the data with cuts (st. dev)	Mean gamma ray energy threshold (TeV)
1979–80	−0.3	1.1	9.3
1982–83	3.1	3.3	4.7
1984–85	1.1	2.9	5.4
Sum	2.6	4.0[a]	

[a] Excess of 421 events over an average background of 10917

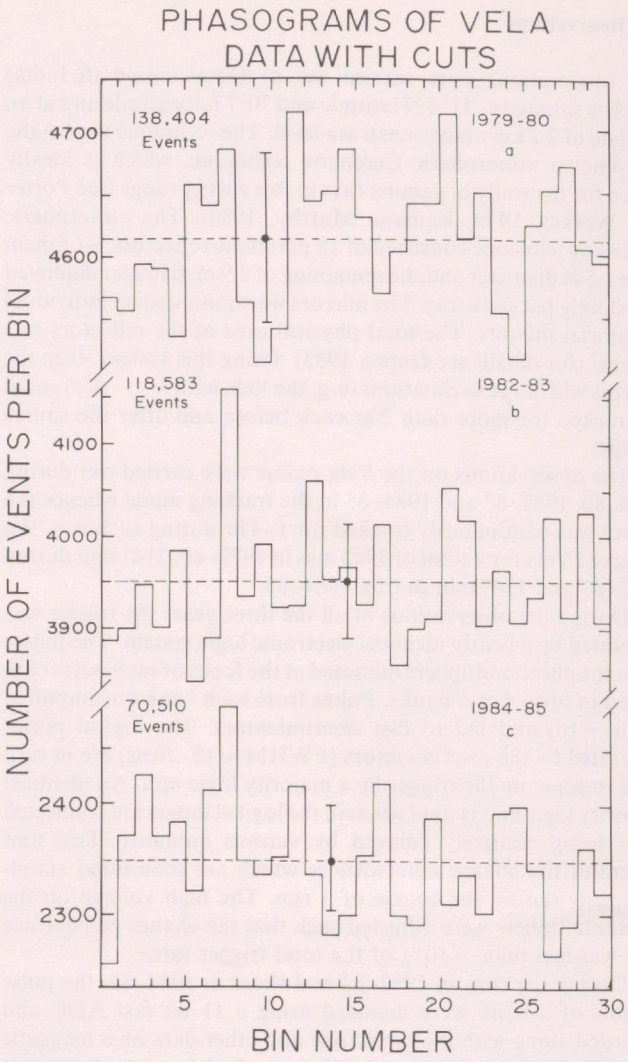

Fig. 3a–c. Phasograms of the 3 data sets after applying cuts to reject higher energy showers: **a** data recorded during 1979–80 while the source hour-angle was such that $|HA| \leqq 20°$. **b** Data recorded during 1982–83 while the source hour-angle eas such that $|HA| \leqq 20°$; and 50% of the lower pulse height showers only are selected. **c** Data recorded during 1984–85 while the source hour-angle was such that $|HA| \leqq 20°$; and 50% of the lower pulse height showers only are selected

double pulse structure probably suggesting that the lower energy events are richer in the signal. From this clue, we tried to select lower energy events based on the pulse height whenever available and/or the source hour-angle. We chose events collected during which the source hour-angle was $|HA| \leqq 20°$. This was applied to all the 3 data sets. However the ADC information on the pulse height was available only for data sets (b) and (c).

In these data only the lower 50% (in energy) of the events are selected and their phasograms derived. The results are shown in Fig. 3. The modified energy thresholds for these subsets (for data taken when $|HA| \leqq 20°$) are 9.3 TeV, 4.7 TeV, and 5.4 TeV respectively. The observed excesses in the expected phase bins are summarised in Table 1 (column 3).

Comparing the results summarized in the table, one can see a marked improvement in the significance of the signal in individual data sets. The phasogram of the sum of the three data sets after applying the aforesaid cuts is shown in Fig. 4. One can see a 4.0σ peak. If one multiplies the individual probabilities of the excesses in all the three phasograms in Fig. 3 separately, assuming that the pulse could be in any of the 30 bins, one gets a chance probability of $2.7\ 10^{-5}$. The number of degrees of freedom used while applying cuts according to the source hour-angle and pulse heights is also accounted for in the above chance probability.

From the observed excess events in the signals tabulated in the table we could calculate the integral photon flux received from this source above the threshold energies shown in the last column. The results are plotted in Fig. 5. The photon energy thresholds are indirectly derived using the event counting rates, average zenith distance of the source and certain inputs from the montecarlo simulation studies of the photon and proton initiated showers. The uncertainties in the input data limit the accuracy of the estimated effective mean energy threshold to be around 50%. The uncertainties in the threshold energy are shown as error bars on the energy axis. Also plotted in the figure are previous measurements of Grindlay et al. (1975). The hatched band shows

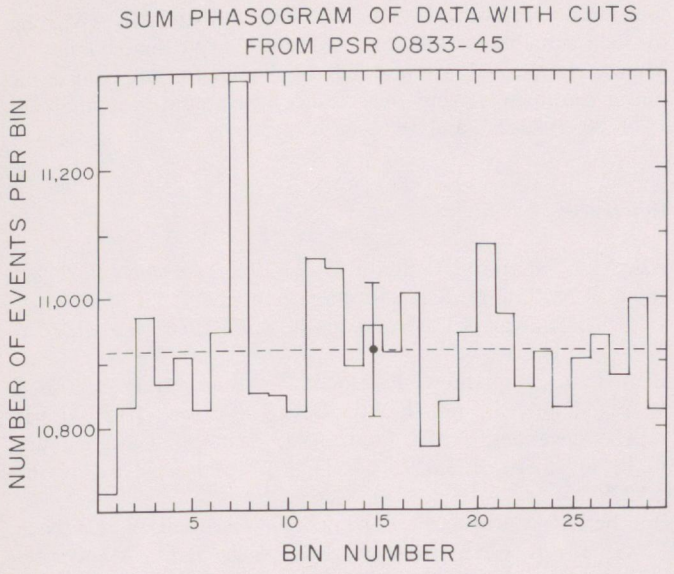

Fig. 4. Sum of all the 3 phasograms shown in Fig. 3

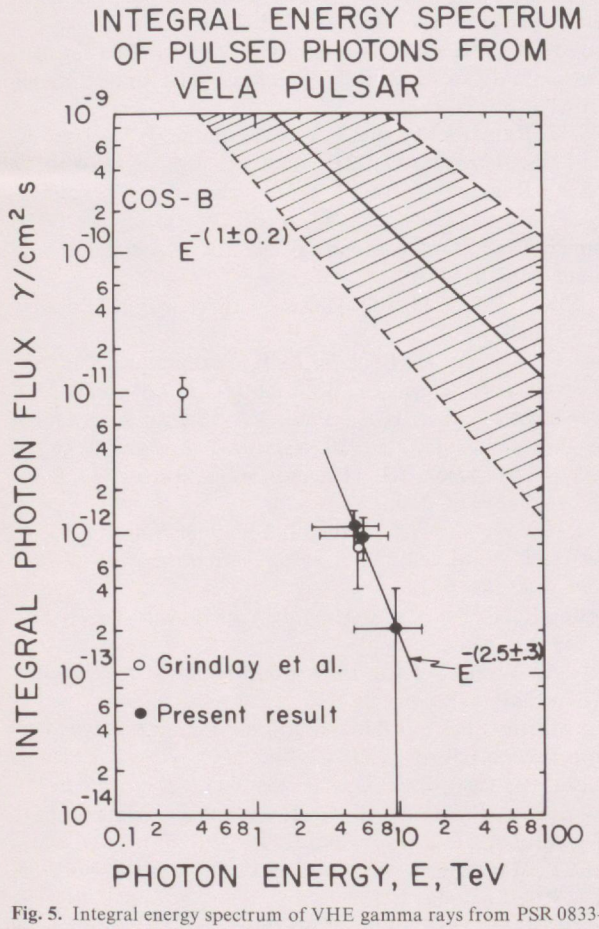

Fig. 5. Integral energy spectrum of VHE gamma rays from PSR 0833–45. The filled circles are from the present results whereas the open circles are the results of an earlier observations by Grindlay et al. (1975). Even though these authors stated that the signals reported were to be considered as upper limits, Grindlay (1982) indicated them as positive fluxes as shown in this figure. The straight line is a least square fit to our measurements and has a slope of $-(2.5\pm 0.3)$.

the extrapolation from the lower energy measurements of COS-B collaboration (Bennett et al., 1977). The results from our previous measurements in 1978–79 (Bhat et al., 1980) and 1980–81 (Gupta et al., 1982) are not plotted in the figure as the absolute phase information was not available during these observations. As one can see in Fig. 5, our present flux estimates are far too low (at least by a factor of ~ 200) compared to the extrapolation from lower energy measurements. The high energy point of Grindlay et al. is in good agreement with the present results.

4. Discussion

The compilation of our measurements of VHE gamma rays from Vela, shows a small but persistent emission in each year at the same phase. The signal strength builds up when the phasograms are summed. However, there is a strong indication that lower energy showers recorded from the direction of the source are richer in the signal. For the events recorded when the source hour-angle was less than 20 degrees on either side of the transit, the mean energy threshold for gamma ray photons reduces by ~ 6–$7\,\%$. However by rejecting $50\,\%$ of the higher energy showers, the threshold energy remains unchanged; but the mean energy of gamma initiated showers falls by a factor of ~ 2.2. By so doing the signal strength improves considerably supporting the evidence of a signal among the lower energy showers.

The position of the signal at the pulsar phase of 0.27 is not totally unexpected. As mentioned in the introduction there is a hint in the lower energy measurements of a persistent excess events at the optical main pulse position (Kanbach et al., 1980). An earlier evidence for the emission of gamma rays of energy >300 GeV by Grindlay et al. (1975) also showed a single pulse at the position of the first optical pulse. In the present case a pulse appears close to the optical phase and there is a hint of a second pulse (at channel nos. 21 and 22) with a characteristic phase difference between the two which is the same as that observed at medium energy range, viz: 0.43. The fact that the main pulses at medium and very high energy gamma ray regions do not agree probably indicates that the mechanisms and sites of production of these gamma rays are different.

It may be recalled that the energy spectrum of medium energy gamma rays in COS-B data were fitted to two different slopes. In the photon energy range 50–300 MeV the best fit value for the slope of the differential spectrum is $-(1.77\pm 0.15)$ while that in the energy range 300–3000 MeV the slope is $-(2.0\pm 0.2)$ (Kanbach et al., 1980). The corresponding slopes of the integral energy spectra would be -0.77 and -1.0 respectively, indicating a trend for a steepening of the energy spectrum with increasing photon energy. The gamma ray energy spectrum shown in Fig. 5 shows that the energy spectrum must steepen either abruptly or continuously in the intervening photon energy range. This again supports the previous conclusion, that their production mechanisms could be different.

On the other hand as the signal to noise ratio improves when relatively higher energy showers are rejected, one can obtain some information regarding the slope of the energy spectrum. According to Vishwanath (1982) the signal to noise ratio is given by:

$$S/N \propto E^{-(\nu_g - \nu_{p/2})},$$

where ν_g and ν_p are the gamma ray and proton integral spectral slopes respectively. Since S/N ratio is increasing when energy is reduced, implies that:

$$\nu_g > \nu_{p/2}.$$

This conclusion is in disagreement with the observation of Grindlay et al. (1975) who found a signal in the highest pulse height group of events. From a fit to the points plotted in Fig. 5 we estimate the slope of the integral gamma ray spectrum to be $-(2.5\pm 0.3)$, consistent with the above lower limit. This is slightly steeper than the value of $v_g = 2.0\pm 0.2$ estimated earlier (Vishwanath, 1982). The error on the slope does not include the uncertainties in the photon energy threshold.

It is interesting to note that association of supernova remnants with isolated pulsars was established in 2 cases: Crab and Vela pulsars. Very high energy (VHE) gamma ray emission has already been seen from Crab pulsar (Gupta et al., 1978; Tumer et al., 1985; Dowthwaite et al., 1984). The present work and the work reported by Grindlay et al. (1975), Grindlay (1982), Gupta et al. (1982) and Bhat et al. (1980), establish that Vela pulsar is also an emitter of VHE gamma rays. Furthermore, it seems to be a more consistent emitter of TeV gamma rays compared to Crab pulsar, since time averaged phasograms from Vela have always shown signals, however weak unlike in the case of Crab pulsar.

It is worth noting here that a model has recently been proposed (Cheng et al., 1986) according to which TeV gamma rays could be produced and emitted without being absorbed in the neutron star magnetosphere of the Vela pulsar. The authors could explain many observed features in the medium energy gamma ray emission. The model predicts the shape of the medium energy gamma ray light curve, the phase at which the main pulse occurs and the phase difference between the main and the interpulse. The model also predicts a double pulse light curve of VHE ($10^{12}-10^{13}$ eV) gamma rays whose total energy is about 10^{-2} of the total slowing down energy. Our results are consistent with these predictions as far as the shape of the light curve is concerned. However the position of the main pulse coincides with that of the optical main pulse rather than that of medium energy gamma rays. It may be noted that whenever a TeV gamma ray signal was detected from this pulsar and whenever the absolute phase information was available, the signal always coincided with the position of the optical main pulse. The fractional energy lost in TeV gamma rays as computed from the present measurements is $1.4\ 10^{-4}$, assuming isotropic emission of gamma rays. Beaming if any will reduce this ratio.

5. Conclusion

The observations in the TeV gamma ray range over 5 yr show small but persistent excess in the phasogram at the same phase. The signal to noise ratio improves significantly when lower energy events are selected. The excess coincides with the optical first pulse position of the pulsar. The integral energy spectrum of the gamma ray signal seen over the years at different energy thresholds exhibits a spectral shape of -2.5. This slope is steeper than that at medium energy gamma ray range. Hence there exists one or more breaks in the energy spectrum between the two energy ranges or there is a continuous steepening of the spectrum as expected on the basis of Compton emission model (like Schlickeiser, 1980; Cheng et al., 1986).

Acknowledgements. It is a pleasure to thank Mr. A.R. Apte for setting up the array and Messers. N.V. Gopalakrishnan, R. Mahalingam, S. Ramani, S. Swaminathan and M. Venkateshwarlu for able maintenance and help in running the experiment. Our thanks are due to Mrs. C.V. Raisinghani and Mr. A.V. John for their valuable assistance in computation. We thank Drs. R.N. Manchester, R.W. Royle and A.R. Klekociuk for supplying us the pulsar parameters from their radio measurements in the year 1979–80, 1982–83, and 1984–85 respectively.

References

Ash, M.E., Shapiro I.I., Smith, W.B.: 1967, *Astrophys. J.* **72**, 338

Bhat, P.N., Gupta, S.K., Ramana Murthy, P.V., Sreekantan, B.V., Tonwar, S.C., Vishwanath, P.R.: 1980, *Astron. Astrophys.* **81**, L3

Bennett, K., Bignami, G.F., Boella, G., Buccheri, R., Hermsen, W., Kanbach, G., Lichti, G.G., Masnou, J.L., Mayer-Hasselwander, H.A., Paul, J.A., Scarsi, L., Swanenburg, B.N., Taylor, B.G., Wills, R.D.: 1977, *Astron. Astrophys.* **61**, 279

Buccheri, R., Caraveo, P., D'Amico, N., Hermsen, W., Kanbach, G., Lichti, G.G., Masnou, J.L., Wills, R.D., Manchester, R.N., Newton, L.M.: 1978, *Astron. Astrophys.* **69**, 141

Cheng, K.S., Ho, C., Ruderman, M.: 1986, *Astrophys. J.* **300**, 522

Dowthwaite, J.C., Harrison, A.B., Kirkman, I.W., Macrae, H.J., McComb, T.J.L., Orford, K.J., Turver, K.E., Walmsley, M.: 1984 *Astrophys. J. Letters* **286**, L35

Grindlay, J.E., Helmken, H.F., Hanbury Brown, R., Davis, J., Allen, L.R.: 1975, *Astrophys. J.* **201**, 82

Grindlay, J.E.: 1982, Proc. Workshop on VHE gamma ray astr. (Ootacamund), p. 257 Eds: Weekes, T.C. and Ramana Murthy, P.V.

Gupta, S.K., Ramana Murthy, P.V., Sreekantan, B.V., Tonwar, S.C.: 1978, *Astrophys. J.* **221**, 268

Gupta, S.K., Ramana Murthy, P.V., Sreekantan, B.V., Tonwar, S.C., Vishwanath, P.R.: 1982, Proc. Workshop on VHE gamma ray astr. (Ootacamund), p. 282 Eds: Weekes, T.C. and Ramana Murthy, P.V.

Gupta, S.K.: 1983, Ph. D. Thesis, University of Bombay (unpublished)

Kanbach, G., Bennett, K., Bignami, G.F., Buccheri, R., Caraveo, P., D'Amico, N., Hermsen, W., Lichti, G.G., Masnau, J.L., Mayer-Hasselwander, H.A., Paul, J.A., Sacco, B., Swanenburg, B.N., Wills, R.D.: 1980, *Astron. Astrophys.* **90**, 163

Knight, F.K., Matteson, J.L., Peterson, L.E., Rothschild, R.E.: 1982, *Astrophys. J.* **260**, 553

Large, M.I., Vaughan, A.E., Mills, B.Y.: 1968, *Nature* **220**, 340

Manchester, R.N., Lyne, A.G.: 1977, *Monthly Notices Roy. Astron. Soc.* **181**, 761

Manchester, R.N. et al.: 1978, *Monthly Notices Roy. Astron. Soc.* **159**, 159

Porter, N.A., Weekes, T.C.: 1979, *Smithsonian Astr. Obs. Spl. Rep.* No. 381

Ramana Murthy, P.V.: 1980, Non-Solar Gamma Rays, Pergamon Press, Oxford, p. 71

Schlickeiser, R.: 1980, *Astrophys. J.* **236**, 945

Thompson, D.J., Fichtel, C.E., Kniffen, D.A., Ogelman, H.B.: 1975, *Astrophys. J. Letters* **200**, L79

Tumer, D.T., Wheaton, W.A., Godfrey, C.P., Lamb, R.C.: 1985, 19th ICRC, La Jolla, **1**, 139

Vishwanath, P.R.: 1982, Proc. Workshop on VHE gamma ray astr. (Ootacamund, eds. T.C. Weekes, P.V. Ramana Murthy, p. 21

Astron. Astrophys. 182, L1–L4 (1987)

ASTRONOMY AND ASTROPHYSICS

LETTER

Letter to the Editor

Hard X-ray observations of the quasar 3C273

S. V. Damle[1], P. K. Kunte[1], S. Naranan[1], B. V. Sreekantan[1], and D. Venkatesan[2]

[1] Tata Institute of Fundamental Research, Bombay 400005, India
[2] Department of Physics, The University of Calgary, Calgary, Alberta, Canada T2N 1N4

Received September 17, 1985; accepted May 12, 1987

SUMMARY

The quasar 3C273 was observed with a balloon-borne phoswich scintillator detector system launched on December 12, 1983 from Hyderabad, India. 3C273 was tracked for 130 minutes and the background was measured in the same ranges of elevation and azimuth when the source was not in the field of view, for approximately the same duration. The fluxes in the 18-25, 25-40, 40-60 and 60-120 keV energy intervals, in units of 10^{-4} photons cm^{-2} s^{-1} kev^{-1} are 11.73 ± 4.20, 2.18 ± 0.64, 1.40 ± 0.29 and 0.30 ± 0.19 respectively. The fluxes above 25 keV are consistent with the balloon observations of 3C273 by Bezler et al., on September 28, 1981 and about thrice as high as the 1978/1979 HEAO-1 measurements. However, our observations taken in conjunction with the lower energy (1-20 keV) data of December 17, 1983 from EXOSAT satellite, indicate possible spectral variations between 1981 and 1983. The implications of these results for astrophysical processes in quasars are discussed.

Key-words:active galactic nuclei - quasars - X-ray sources - 3C273

1. INTRODUCTION

The quasar 3C273, one of the nearest quasars (red shift 0.158), has been extensively studied in all wavelengths of the electromagnetic spectrum, ranging from radio waves of wavelength ~10 cm to gamma rays of energy ~1 GeV. It is the only quasar definitely identified in high energy gamma-rays (30 MeV to 1 GeV) and recent observations cover the near and far infrared and ultraviolet bands as well (see review Ulrich, 1981). Among the remarkable characteristics of 3C273 are the jet, visible in the radio, the optical and the X-ray wavelengths, a small inner jet in mm wavelengths, an apparent superluminal motion of features resolved by VLBI tehniques and a strong anomalous excess ultraviolet radiation. The X-ray spectrum is hard as in most other active galactic nuclei (AGN's). Significant time variations are seen in all wavelengths on time scales of days to years, except in gamma rays. There is in general no clear evidence for any correlated temporal variations in different wavelengths except for con current flaring observed in the infrared to the mm wavelengths (Robson et al., 1983).

Soft X-rays (2-10 keV) from 3C273 were first observed from rockets and subsequently confirmed by the UHURU satellite. X-rays upto 100 keV were detected by OSO-8 and HEAO-1 satellites (Bradt et al., 1979; Worrall et al., 1979; Primini et al., 1979). Balloon measurements of hard X-rays (20-200 keV) were reported by Pietsch et al. (1981) and Bezler et al. (1984). The X-ray spectrum in the 2-10 keV shows no low energy absorption and can be expressed by a power law with index 1.5; the spectrum has a tendency to flatten upto ~30 keV and thereafter steepen (Worrall, 1979). HEAO A4 measurements of 1978 (Primini et al., 1979) in the 20-120 keV range indeed show a steeper spectrum (power law index 1.7). Balloon observations of November 1978 by the AIT/MPE group (Pietsch et al., 1981) in the 20-200 keV range are consistent with the HEAO A4 observations. However the balloon observations of AIT/MPE in September 1981 show a remarkable enhancement by a factor of three in luminosity in 20-200 keV compared to November 1978 and a much flatter spectrum with a power law index 1.2 and no sign of steepening is seen in the spectrum upto 200 keV. In this paper we report a balloon observation of hard X-rays from 3C273 in the 18-120 keV energy lange on December 12, 1983.

2. OBSERVATIONS

Our X-ray telescope consisted of four independent phoswich detectors with 3 mm NaI(Tl) and 25 mm CsI(Na) crystals with good efficiency for detection of X-rays upto 120 keV. The total effective area was 400 cm^2. Each detector was collimated to a field of view of 5° x 5° (FWHM) with slat collimators of copper and surrounded by a passive graded shield of lead, tin and copper to reduce the background. Each phoswich was viewed by a 12.5 cm diameter photomultiplier tube (EMI 9530 or EMI 9618). Non X-ray background counts which appear as coincident Compton-scattered events in both the crystals were rejected by pulse width discrimination (Malkar and Kunte, 1982). Each photon energy was measured in 128 pulse height channels (upto 120 keV) and each pulse width in 128 channels and telemetered to ground. The photon arrival times were measured with a resolution of 0.16 ms. The number of photons in the 120-240 keV energy and above 240 keV were also counted with 5.12 ms time resolution. In-flight calibration was performed periodically by exposing the detectors to an Am^{241} radioactive source to monitor the stability of the detectors and the associated electronics. The orientation of the alt-azimuth mounted telescope was measured by two 10-bit shaft encoders providing an rms accuracy of 0.35° in elevation and azimuth. The residual atmospheric pressure was measured by a pressure transducer (Rosemont 830A3, 0-15 mbar) whose output was fed to a 11-bit A/D converter. Details of the payload and instrumentation have been given by Damle et al. (1986)

Send offprint requests to: S. Naranan

The telescope was flown on December 12, 1983 from Hyderabad, India, (8.5°N geomagnetic latitude), onboard a balloon of volume 1.73 x 10^5 m^3. It floated at an altitude of 36.0 km (4.70 g cm^{-2}) for about 8 hours. The quasar 3C273 (R.A. = $12^h\,26^m$, Dec. = 2.3°) was tracked for 130 minutes in azimuth and elevation from $00^h\,42^m$UT to $02^h\,52^m$UT; this observation was sandwiched between two observations of the background (lasting 72 and 52 minutes) when the telescope scanned the same region of azimuth and elevation but when no known X-ray source was in the field of view. The telescope was oriented by telecommand from ground every two minutes; its pointing accuracy is estimated to be ~0.5°, from ground calibrations and later observations of the bright source Sco X-1 in the same flight. During the observation the measured offset of the telescope varied from 0.7° to 1.8°, the average geometrical efficiency of the telescope being 0.71. The slant atmospheric depth varied from 4.85 to 5.15 mbar during the source observation and from 4.80 to 5.00 mbar during the background measurements. Note that the total background rates measured before and after the 3C273 observation were the same for each detector within 1.0 to 1.5% and the individual channel count rates were also the same within one standard deviation. Background measurements later on in the flight showed similar count rates, indicating that the background is not very sensitive to small variations of ~0.3 mbar in atmospheric depth at ~5 mbar. According to Bezler et al. (1984) the variation of background count rates in their phoswich detectors in the range of 3.1 to 4.2 g cm^{-2} atmospheric depth was never larger than 4%. Pulse width discrimination eliminated nearly 85% of the counts as due to background. The energy resolution for the four detectors ranged from 22% to 40% (FWHM) for 60 keV X-rays from Am^{241}. The background rates at of 4.70 g cm^{-2} at Hyderabad (8.5°N geomagnetic latitude) in units of 10^{-4} counts $cm^{-2}s^{-1}$ keV^{-1} in the energy bands 18-25, 25-40, 40-60, 60-80, 80-100 and 100-120 keV were respectively 6.1, 5.6, 5.1, 5.2, 5.6 and 4.0.

3. DATA ANALYSIS

From 130 minutes of observation of 3C273 and 122 minutes of background measured in the same range of azimuth and elevation, we obtain the net raw count rates attributable to 3C273 in different pulse-height intervals. In Table 1 we give the energy bands corresponding to the chosen pulse height intervals in column 1 and the observed net raw count rates corrected for the average geometrical efficiency of the collimator pointing (0.71) and dead time loss (10%) in column 2. These count rates have to be transformed into X-ray fluxes at the top of the atmosphere after correcting for atmospheric attenuation and detector response function. This was done as follows.

The primary photon number spectrum at the top of the atmosphere assumed to be a power law of the form $AE^{-\gamma}$ photons cm^{-2} s^{-1} keV^{-1}, was transformed into a pulse-height distribution at 5.0 g cm^{-2} (the average slant atmospheric depth in the direction of 3C273), taking into account the variation of atmospheric absorption with energy and the detector response function. The latter included the experimentally determined detector (gaussian) response to monochromatic X-rays and the effects of the escape of iodine K_α and K_β X-rays from the phoswich detector for incident X-rays above the K-electron binding energy. For a given choice of (A,γ), the "expected" count rates were calculated in six pulse-height channels corresponding to energies 18-25, 25-40, 40-60, 60-80, 80-100 and 100-120 keV, for comparison with the observed count rates. To determine the Pearson's χ^2 statistic, the last three channels were combined into a single channel (60-120 keV) because af poor statistics of observation above 60 keV.

The lowest value of χ^2 (4.92 for two degrees of freedom) was obtained for A=0.589 and γ= 2.20; the "expected" values of the count rates for this choice of (A,γ) are given in column 3 of Table 1. Comparing the observed and expected count rates (columns 2 and 3) we note that the maximum contribution to the value is from the 18-25 keV channel. The probability that a power law spectrum can yield a $\chi^2 \geq 4.92$ for two degrees of freedom is 0.085, which is marginally acceptable.

To transform our measurements into primary fluxes at the top of the atmosphere, the most direct method is to multiply the observed count rate (column 2) by the ratio of the theoretical count rate at the top of the atmosphere (calculated according to $AE^{-\gamma}$ with the best fit parameters) to the expected count rate (column 3) in each energy channel. Although the error in γ is large (one sigma error 0.5) it is found that the range of transformed fluxes is within ± 10% of the mean, much less than the statistical errors. The primary fluxes (using γ= 2.20, the best value) are given in the last column of Table 1 and plotted in Fig.1. The errors are statistical. Only for the 18-25 keV flux, an additional 10% error due to uncertainty in atmospheric attenuation is included, the error for higher energy channels being negligible. We estimate the systematic errors of telescope pointing, energy calibration of detectors and conversion of measured count rates to primary fluxes to be smaller than the statistical errors quoted.

Sco X-1 was also observed in the same flight. The results will be reported separately.

4. DISCUSSION

Although the spectral index of 3C273 is poorly determined, the total photon flux in the 18-60 keV X-rays from 3C273 is 1.5 x 10^{-2} photons cm^{-2} s^{-1} with an error of less than 20%. This corresponds to a luminosity L_X (18-60 keV) of (7.09 ± 1.05) x 10^{46} h^{-2} ergs s^{-1} where h is the Hubble constant in units of 50 km s^{-1} Mpc^{-1}. From Fig. 1 we note that our measurements of December 12, 1983 are in good agreement with the AIT/MPE osbervations of September 28, 1981 above 25 keV. In the 18-25 keV energy band our (1983) flux is higher than the AIT/MPE (1981) flux, by about 2.5 standard deviations. We therefore confirm the enhanced flux observed by AIT/MPE in 1981 over the earlier measurement of HEAO A-4 experiment and their own balloon measurements of 1978. Bezler et al. note that the luminosity in 20-200 keV (1981) of (1.2 ± 0.12) x 10^{47} ergs s^{-1} (H=60 km s^{-1} Mpc^{-1} is the highest luminosity observed in any one decade of energy and is comparable to the luminosity attributed to the rest of the entire observed electromagnetic spectrum of 3C273. Interpolating this luminosity (20-200 keV) to 18-60 keV using the spectral index 1.2 quoted by Bezler et al., we get L_X(18-60 keV) = (3.36 ± 0.34) x 10^{46} ergs s^{-1}. Our value L_X(18-60 keV) = (4.92 ± 0.73) x 10^{46} ergs s^{-1} (H = 60 km s^{-1} Mpc^{-1}) is (1.46 ± 0.26) times higher, almost all the excess being accounted for by the higher intensity in the 18-25 keV energy band.

3C273 was also observed by EXOSAT low energy (LE) and medium energy (ME) detectors on December 17, 1983, (Turner et al., 1985) only five days after our hard X-ray measurements. The ME spectrum in the 1-20 keV energy range showed a change in the spectral index from 1.5 ± 0.05 to 0.91 ± 0.13 around 8-10 keV. The highest energy channels in the ME detector

TABLE 1 : 3C273 SPECTRAL DATA OF QUASAR 3C273

Energy Range (keV)	(Observed count rate (cm^{-2} s^{-1})@	Expected* count rate ($cm^{-2}s^{-1}$)@	Source Flux* (ph $cm^{-2}s^{-1}$ keV^{-1})@
18-25	4.50 ± 1.16	2.75	11.70 ± 4.20
25-40	5.80 ± 1.70	8.09	2.18 ± 0.64
40-60	8.95 ± 1.86	7.34	1.40 ± 0.29
60-120	6.59 ± 4.10	7.87	0.30 ± 0.19

@ in units of 10^{-4}

* For primary source spectrum $AE^{-\gamma}$ ph cm^{-2} s^{-1} keV^{-1} with A = 0.589 and γ = 2.20

(around 20 keV) overlap on our lowest energy channel of 18-25 keV. The EXOSAT spectrum below 8 keV (as seen from Fig. 1 of Turner et al., 1985) has a spectral index similar to HEAO-A2 (1978) data shown in our Fig. 1, but with absolute fluxes 1.6 times higher; however it flattens above 8-10 keV up to ~20 keV. At 20 keV the EXOSAT flux of ~8.0 x 10^{-4} photons $cm^{-2}s^{-1}$ keV^{-1} and our flux of (1.17 ± 0.30) x 10^{-3} photons cm^{-2} s^{-1} keV^{-1} are in agreement within one standard deviation. Further, two of our data points - at 25-40 and 40-60 keV - are on the extension of the 2-8 keV EXOSAT spectrum within statistical errors. Assuming that the agreement between EXOSAT and our flux measurements at 20 keV - though obtained from different types of detectors and platforms, but within six days of each other - is not fortuitous, it is reasonable to presume that (1) no change in the intensity of 3C273 in this energy range occurred between the two observations and (2) the enhancement in our 18-25 keV flux compared to the Bezler et al., measurement of 1981 is perhaps real because of the flat spectrum upto 20 keV observed by EXOSAT. These results lead to the following conclusion: the low energy ($\lesssim$10 keV) spectrum (index 1.5) begins to flatten around 8-10 keV (index ~0.9) but is followed by a steepening around 20 keV. Spectra of this kind are predicted by models in which low-frequency black-body radiation is Comptonized in a plasma containing hot Maxwellian electrons (see for example Syunyaev and Titarchuk, 1980; Pozdnyakov, Sobol' and Syunyaev, 1983, the references therein and their Figure 23). Alternately, we can interpret the observed spectra as a superposition of a smooth spectrum of index 1.5 from 2 to 120 keV and an excess flux confined to a narrow range of energy interval around 20 keV.

The Comptonized black-body spectrum has been calculated for a range of plasma electron temperatures (kT_e) and Thompson optical depths τ for electron scattering for spherical and disk-shaped plasmas (Pozdnyakov et al., 1983; Syunyaev and Titarchuk, 1980). The combined EXOSAT and our present data are reasonably well fit by this model with $kT_e \approx 15 \pm 2.5$ keV and $\tau = 4.0 \pm 0.5$ (for disk) or 8 ± 1 (for sphere). Bezler et al. have concluded that kT_e increased from 15 ± 3.5 keV (1978) to >150 keV (1981), the corresponding τ (for spherical gas) being 7.2 ± 0.8 and >1.7 respectively. The hot gas parameters obtained from EXOSAT and our observation (December 1983) are in good agreement with the fit of the HEAO-A2/A4 spectrum by Bezler et al. although the absolute flux values are higher in 1983 by a factor of three. However we wish to exercise a word of caution: combining data from two different types of detectors with different types of corrections for background and atmospheric absorption may be open to question. Thus we consider the above spectral fit as only suggestive of possible significant Comptonization of a low energy thermal component as the source for hard X-rays above 20 keV. Spectral measurements over a wide range of energies, preferably from the same detector are necessary before definitive conclusions can be drawn.

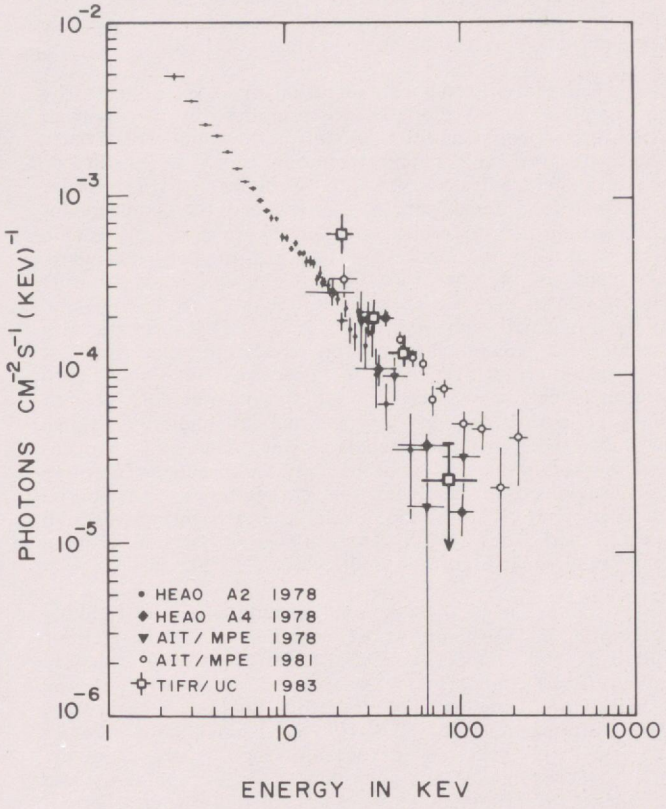

Figure 1. X-ray spectral measurements of quasar 3C273. HEAO-1 A2: Worral et al. (1979): HEAO-1 A4: Primini et al. (1979); AIT/MPE balloon (November 1978): Pietsch et al. (1981); AIT/MPE balloon (September 1981): Bezler et al. (1984). Present measurements are indicated by ⊕. The figure is adapted from Bezler et al. (1984).

Flux variations in 2-17 keV X-rays occured on time scales of several months during 1975-77, when no such variations were apparent in the radio, optical and infrared wavelengths (White and Ricketts, 1979). In the 2-10 keV X-ray observations of Marshall et al., (1981) extending over the years 1975-79, there was an increase in flux by a factor ~2 towards the end of 1979; furthermore on August 30, 1979 the flux increased 1.8 times within 0.5 day. In hard X-rays Worrall et al. (1979) reported a 40% variation of the 2-60 keV X-ray flux on time scale of ~six months in 1976-77 with a characteristic time for temporal variation $t_x = |d \ln F_x / dt|^{-1}$ of 1.5 y. Similar characteristic time t_r in the radio frequencies (ν = 90 GHz) has been reported by Hobbs and Dent (1977). The AIT/MPE observations of November 1978 and September 1981 provide the first evidence for variation in X-rays of 20-200 keV by a factor of three over a period of three years ($t_x \approx$ 3y). After the December 17, 1983 observations already cited, EXOSAT had three more observations in the next six months. In May 1984, the intensity in the 1-10 keV energy range had decreased to about 40% of the December 1983 value and the spectral hardening between 10 and 20 keV was not apparent. Further

the low energy flux (0.1-2 keV) showed intensity and spectral variations between May and June 1984 while the 1-20 keV flux remained the same.

Correlated temporal variations in the radio, X-ray and gamma-ray wavelengths are predicted by non-thermal synchrotron self-Compton models, in which relativisitc electrons producing synchrotron mm radio waves further scatter the radio waves into X-radiation (first order self-Compton, Jones, 1979). There are no simultaneous observations at different wavelengths to test this prediction. In thermal models, a hot gas of non-relativistic electrons of temperature T_e Compton scatters soft photons into X-rays (Katz, 1976; Shakura and Syunyaev, 1976; Lightman and Rybicki, 1979). This process also produces a power law photon spectrum like that of the non-thermal synchrotron process, but only upto photon energies $\sim 3\ kT_e$. All thermal models predict an exponential decline of spectrum at higher energies. In most hot thermal models lower frequency photons and X-ray/gamma-ray photons may be produced in different regions and need not be correlated. The source of soft photons may be inside the scattering medium (Felten and Rees, 1972; Katz, 1976) or outside (Fabian and Rees, 1978; Lightman and Rybicki, 1979).

Since hard X-rays and gamma-rays most likely originate in the inner-most regions of AGN's, their spectral and temporal characteristics are presumably governed by the primary energy source. One of the oft-discussed mechanisms for this source is accretion on to a supermassive (10^6 - 10^9 $M_\odot$) black hole. Power law spectra with no detectable high energy cut-off are observed in AGN's including Seyfert galaxies and quasars. A crucial test to distinguish between thermal and non-thermal models is the spectral shape at energies above 100 keV.

5. CONCLUSION

We have measured the X-ray spectrum of the quasar 3C273 in the 18-120 keV energy range on December 12, 1983. The absolute intensities above 25 keV are consistent with the September 1981 measurements of Bezler et al. (1984) within statistical errors; both are about three times higher than the fluxes observed in November 1978. At 20 keV we obtain a flux higher than that of Bezler et al. (1984) by 2.5 standard deviations. Further, the lower energy (1-20 keV) EXOSAT observations of December 17, 1983, nearly simultaneous with our balloon observations, seem to suggest a flat spectrum in the 10-20 keV energy range, which would imply significant spectral changes between September 1981 and December 1983. None of the hard X-ray measurements of 3C273 or even of other AGN's have clearly revealed an exponential decline of the spectrum at higher energies that is characteristic of all thermal models. Simultaneous observations in the lower (optical, radio) and the higher (X-ray, gamma-ray) frequencies will also provide the means of distinguishing between thermal and non-thermal (synchrotron self-Compton) models. AGN's are the most energetic powerhouses known in astrophysics and their further study in hard X-rays and gamma-rays for spectral and temporal variability are most crucial for a proper understanding of the mechanisms of energy generation.

ACKNOWLEDGEMENTS

This investigation has been made possible by the collaboration between the X-ray Astronomy Group of the Tata Institute of Fundamental Research, Bombay, India and D. Venkatesan, Department of Physics, University of Calgary, Calgary, Alberta, Canada. Support for the participation of Calgary in the form of NSERC grant 69-1565 to D. Venkatesan and large volume balloons provided by the Canadian Centre for Space Science/National Research Council, Ottawa, Canada are acknowledged. We wish to thank the following: R.T. Redkar, R.U. Kundapurkar and the staff of the Balloon Launch Facility, Hyderabad, India for the successful balloon launch; A.T. Kothare, J.P. Malkar, J.G. Devdhekar and S.P. Pawar for building the payload and instrumentation and A.V. John for his help in computation. We wish to acknowledge the useful discussions with R.A. Syunyaev, J. Trümper and W. Pietsch. We thank a referee for drawing our attention to the EXOSAT observations and R. Shafer for his useful comments on the manuscript. D. Venkatesan thanks the Tata Institute of Fundamental Research, for hospitality while in India for the collaborative program. S. Naranan thanks the Max-Planck Institüt für Extraterrestrische Physik, München for its hospitality and the University of Calgary for the visiting scientist award during November-December, 1986.

REFERENCES

Bezler, M., Kendziorra, E., Staubert, R., Hasinger, G., Pietsch, W., Reppin, C., Trümper. J. and Voges, W.: 1984, Astron. Astrophys. 136, 351.

Bradt, H.V., Doxsey, R.E., Johnston, M.D., Schwartz, D.A., Burkhead, M.S. Dent, W.A. Liller, W. and Smith, A.G.: 1979, Astrophys. J. (Lett.) 230, L5.

Damle, S.V., Kunte, P.K., Kothare, A.T., Malkar, J.P., Naranan, S., amd Venkatesan, D.: 1986 in Proc. XXVI COSPAR meeting, Toulouse, France, (in press)

Fabian, A.C. and Rees, M.J.: 1978 in Proc. IAU/COSPAR Symposium on X-ray Astronomy (Eds. Baity. W.A. and Peterson, L.E.) p. 381

Felten, J.E. and Rees, M.J.: 1972, Astron. Astrophys. 17, 226.

Hobbs, R.W. and Dent, W.A.: 1977, A.J., 82, 257

Jones, T.W.: 1979, Astrophys. J. 233, 796.

Katz, J.I.: 1976, Astrophys. J. 206, 910

Lightman, A.P. and Rybicki, G.V.: 1979, Astrophys. J. (Lett), 229, L15.

Malkar, J.P. and Kunte, P.K.: 1982, Nucl. Instr. Meth., 202, 465

Marshall, N., Warwick., R.S. and Pounds, K.A.: 1981, Mon. Not. Roy. Astron. Soc., 194, 987.

Pietsch, W., Reppin, C., Trümper, J. Voges, W., Lewin, W., Kendziorra, E. and Staubert, R.: 1981, Astron. Astrophys., 94, 234.

Pozdnyakov, L.A., Sobol, I.M. and Syunyaev, R.A.: 1983 in: Astrophys. Space Physics Reviews, (Ed. R.A. Syunyaev), 2, p.189.

Primini, F.A., Cooke, B.A., Dobson, C.A., Howe, S.K., Scheepmaker, A., Wheaton, W.A., Lewin, W.H.G., Baity, W.A., Gruber, D.E., Matteson, J.L. and Peterson, L.E.: 1979, Nature, 278, 234.

Robson, E.I., Gear, W.K., Clegg, P.E., Ade, P.A.R., Smith, M.G., Griffin, M.J., Nort, I.G., Radostitz, J.V. and Howard, R.J.: 1983, Nature, 305, 194.

Shakura, N.I. and Syunyaev, R.A.: 1976, Mon. Not. Roy. Astron. Soc., 175, 613.

Syunyaev, R.A. and Titarchuk, L.G.: 1980, Astron. Astrophys., 86, 121.

Turner, M.J.L., Courvoisier, T., Staubert, R., Molteni, D. and Trümper, J.: 1985, Space Sci. Rev. 40, 623

Ulrich, R.H.: 1981, Space Sci. Rev. 28, 89.

White, G.J. and Ricketts, M.J.: 1979, Mon. Not. Roy. Astron. Soc., 175, 613

Worrall, D.M., Mushotzky, R.F., Boldt, E.A., Holt, S.S. and Serlemitsos, P.J.: 1979, Astrophys. J., 232, 683

ERRATUM

The present measurements of fluxes from 3C273 (⊹ TIFR/UC 1983) are plotted incorrectly in Fig 1, page L3. The correct figure appears below. The figure caption is unaltered. The correct fluxes appears in Table on page L3.

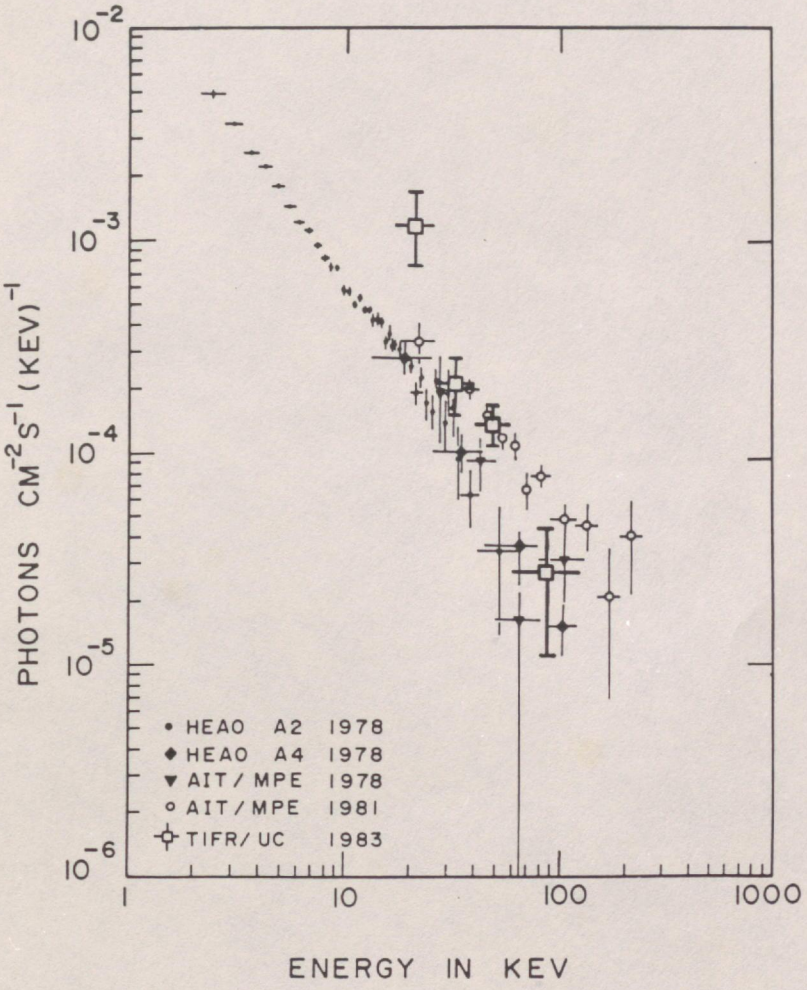

Figure 1. X-ray spectral measurements of quasar 3C273. HEAO-1 A2: Worral et al. (1979): HEAO-1 A4: Primini et al. (1979); AIT/MPE balloon (November 1978): Pietsch et al. (1981); AIT/MPE balloon (September 1981): Bezler et al. (1984). Present measurements are indicated by ⊹ . The figure is adapted from Bezler et al. (1984).

Astron. Astrophys. 186, L20 (1987)

ASTRONOMY AND ASTROPHYSICS

Erratum

Hard X-ray observations of the quasar 3C273

S. V. Damle[1], P. K. Kunte[1], S. Naranan[1], B. V. Sreekantan[1], and D. Venkatesan[2]

[1] Tata Institute of Fundamental Research, Bombay 400005, India
[2] Department of Physics, The University of Calgary, Calgary, Alberta, Canada T2N 1N4

Astron. Astrophys. 182, L1–L4 (1987) *(Letter to the Editor)*

When the manuscript of this Letter was sent to press at the beginning of July, an older version Fig. 1 had been erroneously included on page L3. The correct version of Fig. 1 is printed here. The caption, which remains unchanged, is also included for convenience.

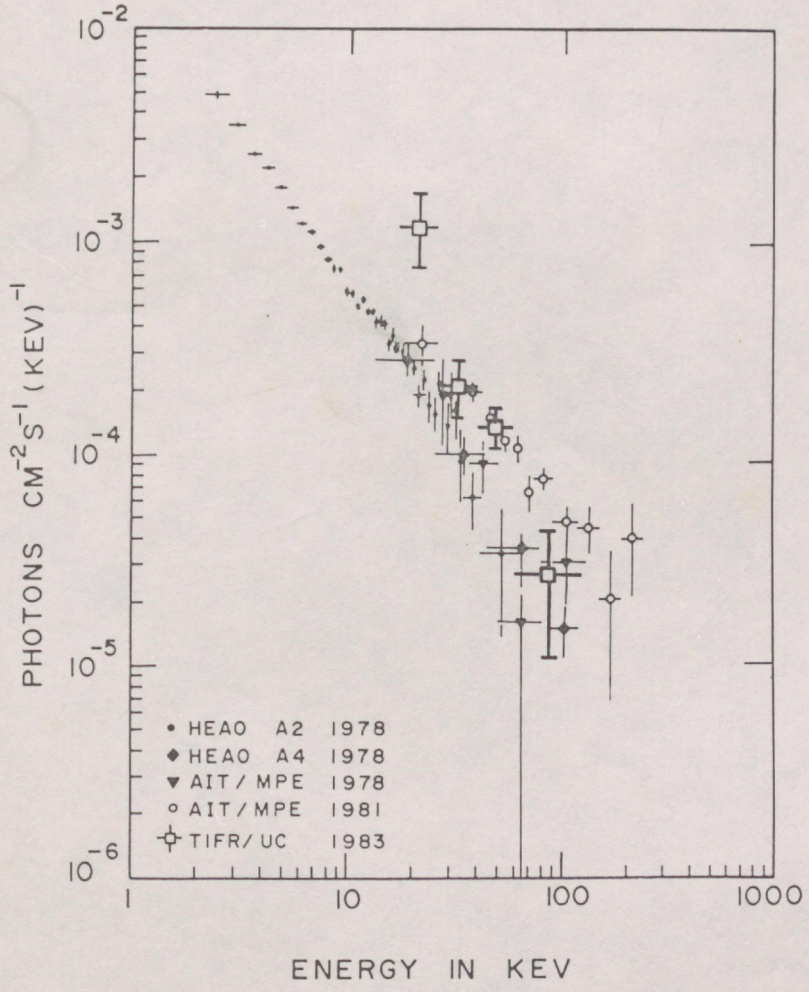

Fig. 1. X-ray spectral measurements of quasar 3C273. HEAO-1 A2: Worral et al. (1979); HEAO-1 A4: Primini et al. (1979); AIT/MPE balloon (November 1978): Pietsch et al. (1981); AIT/MPE balloon (September 1981): Bezler et al. (1984). Present measurements are indicated by ⊕. The figure is adapted from Bezler et al. (1984)